The linear stability of a ridge of fluid subject to a jet of air

I. S. McKinley and S. K. Wilson*

Department of Mathematics, University of Strathclyde,

Livingstone Tower, 26 Richmond Street,

Glasgow G1 1XH, United Kingdom.

(March 12th, 1999. Third Revision October 16th, 2000)

Abstract

In this paper we investigate the linear stability of an initially symmetric two-dimensional thin ridge of Newtonian fluid of finite width on a horizontal planar substrate acting under the influence of a symmetric two-dimensional jet of air normal to the substrate. Ridges both with and without a dry patch at their centre are considered. For both problems we examine both the special case of quasi-static motion (corresponding to zero capillary number) analytically and the general case of non-zero capillary number numerically. In all cases the ridge is found to be unconditionally unstable, but the nature and location of the most unstable mode are found to depend on the details of the specific problem considered.

---

*Corresponding author. Telephone +44(0)141-548-3820, Fax +44(0)141-552-8657, Email `s.k.wilson@strath.ac.uk`

I. INTRODUCTION

Because of the numerous technological processes and natural situations in which they play an important role, the dynamics of thin fluid films have received considerable theoretical and experimental attention in recent years (see, for example, the recent review articles by Oron *et al.*[1] and Myers[2]). However, despite its considerable technological relevance, the situation in which the film is subject to an externally imposed force has received relatively little attention thus far. In the present work we shall consider one practically important example of this kind of problem, namely an initially symmetric two-dimensional ridge of fluid of finite width subject to a jet of air.

There have been a few previous studies of problems of this kind. Moriarty *et al.*[3] considered the unsteady spreading of a two-dimensional drop of fluid under the action of a jet of air blowing either vertically downwards onto the substrate or parallel to it. In the first case, the jet was modelled as a parabolic pressure distribution in the air, and the shear stress at the free surface of the fluid caused by the air flow was neglected, while in the second case the jet was modelled as a constant shear stress distribution at the free surface of the fluid while the variations in the air pressure were neglected. In both cases unsteady solutions were obtained both numerically and analytically in the asymptotic limit of weak surface tension. King *et al.*[4] studied steady two-dimensional periodic waves on a fluid film on an inclined plane caused by a jet of air flowing upwards over it. Their model allowed the external pressure gradient to depend on the shape of the free surface of the film, but assumed that the shear stress at the free surface was constant. King and Tuck[5] studied the corresponding problem for a ridge of fluid of finite width on an inclined plane and found that steady solutions are possible only if the angle of inclination of the plane to the horizontal is sufficiently small and that below this critical value two steady solutions exist for each inclination angle. Recently, McKinley *et al.*[6] studied the unsteady spreading of a drop due to a jet of air acting normally to the substrate. The jet of air was modelled as a parabolic pressure distribution, and sessile, pendent and zero-gravity situations were all considered.

Both symmetric two-dimensional and axisymmetric three-dimensional problems were solved in the quasi-static limit of small capillary number for both an "annular" drop with a dry patch at its centre and a "non-annular" drop without a dry patch.

Much of the other work that has been done on problems of this kind is motivated by the so-called "jet-stripping" or "air-knife" industrial coating process in which the thickness of a fluid film on a moving substrate is controlled by blowing a jet of air onto the film. For example, the pioneering steady two-dimensional analysis of Thornton and Graff[7] (subsequently extended and clarified by Tuck[8]) was generalised by Ellen and Tu[9] to include a non-zero shear stress at the free surface and by Tuck and Vanden-Broeck[10] to include surface tension. Recently Kriegsmann *et al.*[11] investigated the effect of a steadily-moving exponential pressure distribution on a fluid film on an inclined plane and found that there is a finite range of values of the capillary number in which no steady solution exists and unsteady solutions develop shock-like free-surface profiles.

The general issue of the stability of thin fluid films has received considerable attention in recent years, much of it motivated by the well-known "fingering" instability that often develops at the leading edge of a thin film draining down an inclined plane. The linear stability of the initially two-dimensional "capillary ridge" that can develop near the leading edge in this situation was first studied theoretically by Troian *et al.*[12] who showed that the ridge is always unstable to sufficiently long-wavelength transverse perturbations. Troian *et al.*[12] also showed that their theoretical prediction for the (finite) most unstable wavelength is in good agreement with their experimental results. This pioneering analysis has subsequently been re-examined and generalised by several authors, including Spaid and Homsy[13], Bertozzi and Brenner[14], López *et al.*[15,16] and Kataoka and Troian[17,18]. The linear stability and nonlinear evolution of an initially two-dimensional ridge of finite width on an inclined plane was analysed by Hocking[19] and Hocking and Miksis[20]. In particular, this work shows that while a linear stability analysis of quasi-static motion with prescribed contact-angle variation predicts that the ridge is most unstable to long-wavelength transverse perturbations, relaxing these assumptions means that the most unstable wavelength is finite for all but unreasonably

small values of the slip length at the solid/fluid interface. Aspects of the linear stability and non-linear evolution of a hole in a thin fluid layer have been investigated by Moriarty and Schwartz[21], Wilson and Terrill[22] and López *et al.*[23].

In this paper we investigate the linear stability of an initially symmetric two-dimensional thin ridge of Newtonian fluid of finite width on a horizontal planar substrate acting under the influence of a symmetric two-dimensional jet of air normal to the substrate. Both "annular" (with a dry patch at its center) and "non-annular" (without a dry patch) ridges are considered. For both problems we confirm and extend the analytical results of McKinley *et al.*[6] in the special case of quasi-static motion (corresponding to zero capillary number) and investigate numerically the general case of non-zero capillary number. Finally, we offer a physical interpretation of our results.

II. PROBLEM FORMULATION

Consider an initially two-dimensional ridge of incompressible Newtonian fluid of finite width with constant viscosity μ, density ρ and surface tension τ on a solid horizontal planar substrate in the presence of a symmetric two-dimensional jet of air. We employ Cartesian coordinates (x, y, z) chosen so that the substrate is given by $z = 0$ and the z, y plane is the symmetry plane of the jet. With respect to these coordinates the thickness of the fluid film is denoted by $z = h(x, y, t)$ and the velocity and pressure of the fluid by $\mathbf{u} = \mathbf{u}(x, y, z, t)$ and $p = p(x, y, z, t)$ respectively. In this paper we shall consider only ridges that are initially symmetric with respect to the symmetry plane of the jet. For a "non-annular" ridge without a dry patch at its center the positions of the contact lines are denoted by $x = R_1(y, t)$ at which the contact angle is $\phi = \phi(t)$ and $x = R_2(y, t) > R_1$ at which the contact angle is $\theta = \theta(t)$, where t denotes time. For an "annular" ridge with a dry patch at its centre we can without loss of generality restrict our attention to the part of the ridge lying in $x \geq 0$, and so we need only consider the case $R_1 > 0$. We model the jet with a parabolic pressure distribution in the air given by $p = p_0 - kx^2/2$, where p denotes the pressure, p_0 is the

maximum value of the air pressure at $x = 0$ and k is a positive constant. The shear stress at the free surface caused by the jet is neglected. The geometry of the non-annular problem is shown in Fig. 1.

We follow the approach pioneered by Greenspan[24], Ehrhard and Davis[25], and Anderson and Davis[26] and assume that the speeds of the contact lines are related to their contact angles by the "Tanner Laws"

$$(R_1)_t = \kappa(\phi_0^m - \phi^m), \tag{1}$$

$$(R_2)_t = \kappa(\theta^m - \theta_0^m), \tag{2}$$

where ϕ_0 and θ_0 are the equilibrium contact angles and κ is an empirically-determined positive constant with dimensions of velocity. More general Tanner Laws have been used by McKinley *et al.*[6]. It should, however, be noted that this is not the only possible way of modelling the behaviour near the contact line. For example, Hocking[27,28] proposes an alternative formulation in which the microscopic contact angle always takes its constant static value and from which the observed variation of the macroscopic contact angle can be predicted. In the case $m = 3$ the two approaches yield the same qualitative results and Hocking[28] finds that the alternative approach is in better quantitative agreement with the experimental data of Anderson and Davis[26] for a droplet of water. When $\phi_0 \neq \theta_0$ the static contact angles at the two contact lines are different, a somewhat artificial situation which (as McKinley *et al.*[6] pointed out) could, however, occur if the substrate is inhomogeneous with an appropriate change of physical properties somewhere in $R_1 < x < R_2$.

Provided that inertia effects are negligible (i.e. provided that the appropriate Reynolds number is sufficiently small) and that the ridge is sufficiently thin in the direction normal to the substrate, the familiar lubrication approximation to the governing Navier-Stokes and mass conservation equations yield

$$0 = p_z + \rho g, \tag{3}$$

$$\mu u_{zz} = p_x, \tag{4}$$

$$\mu v_{zz} = p_y, \tag{5}$$

$$u_x + v_y + w_z = 0, \tag{6}$$

where g denotes acceleration due to gravity, subject to the boundary conditions

$$u = \lambda u_z, \quad v = \lambda v_z \quad \text{on} \quad z = 0, \tag{7}$$

$$\mu u_z = 0, \quad \mu v_z = 0 \quad \text{on} \quad z = h, \tag{8}$$

$$p = p_0 - \frac{kx^2}{2} - \tau \nabla^2 h \quad \text{on} \quad z = h, \tag{9}$$

$$w = h_t + u h_x + v h_y \quad \text{on} \quad z = h, \tag{10}$$

where the fluid velocity has been written $\mathbf{u}=(u, v, w)$. Equation (7) is the slip condition with slip length $\lambda = \lambda(h)$ that mitigates the stress singularity at the contact line. Equation (8) represents zero tangential stress at the free surface and Eq. (9) is the normal stress condition which includes both the effects of surface tension and the non-uniform external pressure loading caused by the jet of air. Equation (10) is the kinematic free-surface condition which can be re-written in the form

$$h_t + \nabla \cdot (Q_1, Q_2) = 0, \tag{11}$$

where Q_1 and Q_2 denote the fluxes in the x and y directions respectively defined by

$$Q_1 = \int_0^h u \, \mathrm{d}z \quad \text{and} \quad Q_2 = \int_0^h v \, \mathrm{d}z. \tag{12}$$

Solving Eqs. (3) – (10) for u and v allows Q_1 and Q_2 to be evaluated explicitly, and substituting these expressions into Eq. (11) gives the governing equation for h.

We non-dimensionalise the problem using a characteristic horizontal length scale L (to be defined subsequently) and κ as the characteristic horizontal velocity scale. The corresponding non-dimensional variables are defined by $x = Lx'$, $y = Ly'$, $h = \theta_0 L h'$, $R_1 = \theta_0^m L R_1'$, $R_2 = \theta_0^m L R_2'$, $t = Lt'/\kappa$, $\phi = \theta_0 \phi'$, $\phi_0 = \theta_0 \phi_0'$ and $\theta = \theta_0 \theta'$. Dropping the primes at once for simplicity we obtain the non-dimensional version of the governing equation for h, namely

$$C h_t + \nabla \cdot \left[h^2 \left(\frac{h}{3} + \lambda \right) \nabla \left(\nabla^2 h - G^2 h + \frac{J x^2}{2} \right) \right] = 0, \tag{13}$$

together with the non-dimensional versions of Eqs. (1) and (2), namely,

$$(R_1)_t = \phi_0^m - \phi^m, \tag{14}$$

$$(R_2)_t = \theta^m - 1, \tag{15}$$

where the constant $J = kL^3/\tau\theta_0$ is a non-dimensional measure of the jet strength, $C = \kappa\mu/\tau\theta_0^3$ is the (mobility) capillary number and $G^2 = \rho g L^2/\tau$ is the Bond number. The appropriate boundary conditions for Eq. (13) are

$$h(R_1, y, t) = 0, \tag{16}$$

$$h(R_2, y, t) = 0, \tag{17}$$

$$(h_x - (R_1)_y h_y)(1 + (R_1)_y^2)^{-1/2}|_{x=R_1} = \phi, \tag{18}$$

$$(h_x + (R_2)_y h_y)(1 + (R_2)_y^2)^{-1/2}|_{x=R_2} = -\theta, \tag{19}$$

which must be satisfied together with appropriate initial conditions for h, R_1 and R_2. Equations (16) and (17) require the free surface to have zero height at the contact lines while Eqs. (18) and (19) ensure that the contact angles take the correct values. The volume of a non-annular ridge or the semi-volume of an annular ridge in a width $2d$ is given by

$$2dV = \int_{-d}^{d}\int_{R_1}^{R_2} h \, \mathrm{d}x\mathrm{d}y. \tag{20}$$

Without loss of generality we can choose $L = (\tau\theta_0/k)^{1/3}$ (corresponding to setting $J = 1$). For clarity we shall retain J explicitly in all of our analytical calculations but set $J = 1$ in all of our numerical calculations.

For simplicity we shall hereafter restrict our attention to the special case of sufficiently narrow ridges in which gravity effects are negligible, and hence set $G = 0$. In principle, all the subsequent calculations could be repeated with gravity effects included (just as McKinley *et al.*[6] did in their quasi-static analysis), but since our preliminary calculations revealed no qualitatively new phenomena for non-zero values of G^2 we do not pursue this point further in the present study.

Haley and Miksis[29] undertook a detailed study of droplet spreading for various combinations of slip law and contact-line condition and found that, while there are significant differences between the different cases (for example, in the spreading rates and the details of the behaviour of h near the contact line), the qualitative features of the droplet motion are the same in all the cases they considered. In the absence of any general agreement about the correct form of the slip law or Tanner law, we adopt the simple Navier slip model in which λ is a constant (as used, for example, by Hocking[19]), and the linear Tanner Laws obtained by setting $m = 1$ in Eqs. (14) and (15) (as used, for example, by Greenspan[24]).

A. Basic State

In equilibrium $h(x, y, t) = h_0(x)$, $R_1(y, t) = R_1^0$, $R_2(y, t) = R_2^0$, $\theta = 1$ and $\phi = \phi_0$. Substituting these expressions into Eqs. (13), (16), (17) and (19) with $G = 0$ yields the governing equation for the basic-state profile, namely

$$h_0''' + Jx = 0, \tag{21}$$

where the prime denotes differentiation with respect to x, subject to the boundary conditions

$$h_0(R_1^0) = 0, \tag{22}$$

$$h_0(R_2^0) = 0, \tag{23}$$

$$h_0'(R_2^0) = -1. \tag{24}$$

The solution for h_0 is given by

$$h_0 = (R_2^0 - x)(x - R_1^0)\left\{\frac{J}{24}[x^2 + (R_1^0 + R_2^0)x - R_2^0(2R_2^0 + R_1^0)] + \frac{1}{R_2^0 - R_1^0}\right\}. \tag{25}$$

From Eq. (20) the volume of the ridge is given by

$$V = \frac{1}{6}(R_2^0 - R_1^0)^2 - \frac{J}{360}(R_2^0 - R_1^0)^4(2R_1^0 + 3R_2^0), \tag{26}$$

while from the remaining boundary condition Eq. (18) we obtain the relationship between ϕ_0, R_1^0 and R_2^0, namely

$$\phi_0 = 1 - \frac{J}{12}(R_2^0 + R_1^0)(R_2^0 - R_1^0)^2. \tag{27}$$

B. Linear Stability Problem

In order to analyse the linear stability of the ridge to small transverse perturbations with wavenumber q we write $h = h_0(x) + h_1(x)\exp(iqy + \sigma t)$, $R_1 = R_1^0 + R_1^1 \exp(iqy + \sigma t)$ and $R_2 = R_2^0 + R_2^1 \exp(iqy + \sigma t)$, where $h_1(x)$ is the perturbation to the basic-state profile, R_1^1 and R_2^1 are the perturbations to the positions of the contact lines and σ is the unknown (complex) growth coefficient. Substituting these expressions into Eqs. (13) – (19) and retaining only first-order terms in the perturbations yields the governing equation for h_1:

$$3C\sigma h_1 + \left[h_0^2(h_0 + 3\lambda)(h_1'' - q^2 h_1)'\right]' - q^2 h_0^2(h_0 + 3\lambda)(h_1'' - q^2 h_1) = 0, \tag{28}$$

which is subject to the boundary conditions

$$R_1^1 = -\frac{1}{\phi_0} h_1(R_1^0), \tag{29}$$

$$R_2^1 = h_1(R_2^0), \tag{30}$$

$$h_1'(R_1^0) + h_0''(R_1^0) R_1^1 = -\sigma R_1^1, \tag{31}$$

$$h_1'(R_2^0) + h_0''(R_2^0) R_2^1 = -\sigma R_2^1. \tag{32}$$

Eliminating R_1^1 and R_2^1 from Eqs. (29) – (32) and using Eq. (25) yields

$$\phi_0 h_1'(R_1^0) - f_1(J, R_1^0, R_2^0) h_1(R_1^0) = \sigma h_1(R_1^0), \tag{33}$$

$$h_1'(R_2^0) + f_2(J, R_1^0, R_2^0) h_1(R_2^0) = -\sigma h_1(R_2^0), \tag{34}$$

where the functions $f_1(J, R_1^0, R_2^0)$ and $f_2(J, R_1^0, R_2^0)$ are given by

$$f_1(J, R_1^0, R_2^0) = \frac{J}{12}(R_2^0 - R_1^0)(5R_1^0 + 3R_2^0) - \frac{2}{R_2^0 - R_1^0}, \tag{35}$$

$$f_2(J, R_1^0, R_2^0) = \frac{J}{12}(R_1^0 - R_2^0)(R_1^0 + 3R_2^0) - \frac{2}{R_2^0 - R_1^0}. \tag{36}$$

As Hocking and Miksis[20] point out, in the special case $q = 0$ (but not otherwise) it is also necessary to impose in addition the volume condition

$$\int_{R_1^0}^{R_2^0} h_1 \mathrm{d}x = 0. \tag{37}$$

III. THE NON-ANNULAR RIDGE ($\phi_0 = 1$)

A. Basic State

Seeking an initially symmetric non-annular solution by setting $R_0 = -R_1^0 = R_2^0$ in Eq. (27) yields $\phi_0 = 1$ (so that the two basic-state contact angles are equal). From Eq. (25) we obtain the basic-state profile

$$h_0 = \frac{1}{24R_0}(x^2 - R_0^2)\left[JR_0(R_0^2 - x^2) - 12\right], \tag{38}$$

and from Eq. (26) the volume of the ridge is given by

$$V = \frac{2}{45}R_0^2(15 - JR_0^3). \tag{39}$$

Figure 2 plots basic-state profiles for $R_0 = 0.6$, 1, 1.4, 1.8 and 2.2. These solutions are exactly the two-dimensional non-annular solutions described by McKinley *et al.*[6]. Note that "physical" solutions (i.e. solutions for which $h_0 \geq 0$ over the entire interval $-R_0 \leq x \leq R_0$) exist only when R_0 lies in the range $0 \leq R_0 \leq (12/J)^{1/3}$. When $R_0 > (12/J)^{1/3}$ Eq. (38) predicts that $h < 0$ at $x = 0$, motivating the study of an annular ridge in section IV.

B. Linear Stability Problem

The governing equation for h_1 is given by Eq. (28) subject to the boundary conditions

$$h_1'(-R_0) + \left(\frac{JR_0^3 + 3}{3R_0}\right) h_1(-R_0) = \sigma h_1(-R_0), \tag{40}$$

$$h_1'(R_0) - \left(\frac{JR_0^3 + 3}{3R_0}\right) h_1(R_0) = -\sigma h_1(R_0). \tag{41}$$

As we have already seen, in the special case $q = 0$ it is also necessary to impose the volume condition

$$\int_{-R_0}^{R_0} h_1 \mathrm{d}x = 0. \tag{42}$$

C. Quasi-Static Motion $C = 0$

We can make considerable analytical progress in the special case $C = 0$. In this case the bulk of the ridge instantaneously adopts a quasi-static shape whose subsequent motion is entirely determined by the Tanner laws given in Eqs. (14) and (15) (see, for example, Oron *et al.*[1]). Note that all the analytical results presented here have been confirmed by numerical calculations of the kind described in the next section.

1. Two-Dimensional Perturbations $q = 0$

Substituting $C = 0$ and $q = 0$ into Eq. (28) and integrating once yields

$$h_0^2(h_0 + 3\lambda)h_1''' = Q^*, \tag{43}$$

where Q^* is a constant. The general solution of Eq. (43) can be written in the form

$$h_1 = Q^* f(x, J, R_0) + \alpha x^2 + \beta x + \gamma, \tag{44}$$

where α, β and γ are constants and the function $f(x, J, R_0)$ is not given here explicitly for brevity. As $x \to R_0^-$, $f(x, J, R_0) \sim (R_0 - x)\ln(R_0 - x)/3\lambda$ and so solutions for h_1 that do not have a singularity at $x = R_0$ are possible only if $Q^* = 0$. Thus the appropriate solution for h_1 is simply

$$h_1 = \alpha x^2 + \beta x + \gamma, \tag{45}$$

and imposing the volume condition (42) on Eq. (45) yields $\alpha = -3\gamma/R_0^2$. Evidently the solutions for h_1 can be either symmetric or antisymmetric. For symmetric solutions ($\beta = 0$) applying the boundary condition (41) to Eq. (45) yields $\sigma = \sigma_{s0}$, where

$$\sigma_{s0} = \frac{JR_0^3 - 6}{3R_0}, \tag{46}$$

recovering the expression for the growth rate of the symmetric mode first obtained by McKinley *et al.*[6]. For antisymmetric solutions ($\alpha = \gamma = 0$) applying the boundary condition (41) to Eq. (45) yields $\sigma = \sigma_{a0}$, where

$$\sigma_{a0} = \frac{JR_0^2}{3} > 0. \tag{47}$$

Figure 3 plots σ_{s0} and σ_{a0} as functions of R_0. Since $\sigma_{a0} > \sigma_{s0}$ and $\sigma_{a0} > 0$ the conditionally stable symmetric mode considered by McKinley *et al.*[6] is always more stable than the unconditionally unstable antisymmetric mode obtained here for the first time. Note that in the special case when the air jet is absent ($J = 0$) the symmetric mode is always stable, while the antisymmetric mode (which simply corresponds to a translation of the initial profile) is neutrally stable.

2. Three-Dimensional Perturbations $q > 0$

In the general case $q > 0$ a solution of Eq. (28) for h_1 with $C = 0$ that does not have a singularity at $x = R_0$ is given by

$$h_1 = \alpha \cosh(qx) + \beta \sinh(qx), \tag{48}$$

where α and β are constants. Again, the solutions for h_1 can be either symmetric or antisymmetric. The growth rate of symmetric modes ($\beta = 0$) is given by

$$\sigma_s = \frac{JR_0^3 + 3}{3R_0} - q \tanh(qR_0). \tag{49}$$

Note that $\sigma_s \to \hat{\sigma}_{s0}$ as $q \to 0$, where $\hat{\sigma}_{s0} = (JR_0^3 + 3)/3R_0 \neq \sigma_{s0}$, i.e. because these solutions do not satisfy the volume condition (42) for $q > 0$ we do not recover the solution obtained previously in the case $q = 0$ in the limit $q \to 0$. The growth rate of antisymmetric modes ($\alpha = 0$) is given by

$$\sigma_a = \frac{JR_0^3 + 3}{3R_0} - q \coth(qR_0). \tag{50}$$

Note that $\sigma_a \to \hat{\sigma}_{a0}$ as $q \to 0$, where $\hat{\sigma}_{a0} = JR_0^2/3 = \sigma_{a0}$, i.e. because these solutions do satisfy the volume condition (42) for all $q > 0$ we recover the solution obtained previously in the case $q = 0$ in the limit $q \to 0$. The neutral stability curves for $q > 0$ obtained by setting $\sigma_s = 0$ and $\sigma_a = 0$ in Eqs. (49) and (50) respectively are plotted in Fig. 4.

Figures 5(a) and (b) plot the growth rates σ_s and σ_a as functions of $q \geq 0$ for $R_0 = 1$ and 2.2 respectively. Symmetric modes are denoted by solid lines and antisymmetric modes by dashed lines. At $q = 0$, a filled circle denotes a solution, an empty circle no solution. Note that the lower filled circle corresponds to σ_{s0}, i.e. to the symmetric mode obtained by McKinley *et al.*[6]. Since $\sigma_s > \sigma_a$ for $q > 0$, both σ_s and σ_a are monotonically decreasing functions of q for all $q > 0$, $\hat{\sigma}_{s0} > \hat{\sigma}_{a0} = \sigma_{a0} > \sigma_{s0}$ and $\hat{\sigma}_{s0} > 0$, we deduce that long-wavelength symmetric modes with growth rate approaching $\hat{\sigma}_{s0}$ in the limit $q \to 0$ are always the most unstable when $C = 0$. Note that in the special case $J = 0$ all anti-symmetric and sufficiently short-wavelength symmetric modes are stable, but sufficiently long-wavelength symmetric modes are unstable.

D. The General Case $C \neq 0$

In the general case $C \neq 0$ the bulk of the ridge responds on a timescale of C and so the motion is always retarded relative to the case $C = 0$. To obtain the neutral stability curves for $C \neq 0$ we set $\sigma = 0$ in Eq. (28) and the boundary conditions (40) and (41). This procedure yields the same neutral stability curves as those calculated previously in the case $C = 0$ as shown in Fig. 4. When $\sigma \neq 0$ we must proceed numerically.

1. Numerical Procedure

A FORTRAN code was written to solve the eigenvalue problem given by Eq. (28) and the boundary conditions (40) and (41) numerically using finite differences. The details of this numerical procedure are summarised below; further details are given by McKinley[30].

An uneven grid of $N + 1$ points, x_i for $i = 0, \ldots, N$, is used in the calculations and is chosen so that the grid points are clustered towards the contact lines. This is achieved using the weighting function described by Vinokur[31], where an even grid u_i for $i = 0, \ldots, N$, is transformed to an uneven grid x_i for $i = 0, \ldots, N$, by the relation

$$x_i = R_0 \left(\frac{\tanh[(u_i - 1/2)c]}{\tanh(c/2)} \right) \quad \text{for } i = 0, \ldots, N, \tag{51}$$

where the user is free to choose the value of the stretching parameter c. Calculating the finite difference weights is carried out automatically using a very efficient algorithm developed by Fornberg[32]. For a given (not necessarily regular) set of grid points x_i for $i = 0, \ldots, N$, the point at which approximations are desired $x = \xi$ (not necessarily a grid point) and highest order of derivative of interest K, Fornberg's[32] algorithm calculates weights d_{ij}^k such that the approximations

$$\left. \frac{\partial^k f}{\partial x^k} \right|_{x=\xi} \simeq \sum_{j=0}^{i} d_{ij}^k f(x_j), \quad k = 0, \ldots, K, \;\; i = k, \ldots, N,$$

are all optimal in the sense that they permit the maximum order of approximation possible for a stencil consisting of $i+1$ points. In the present application we require approximations at the grid points only and we will only apply the algorithm to a subset of the domain, the number of nodes in a particular stencil depending on the required order of approximation to the derivative, I, and on the order of the derivative to be approximated, k. Specifically, the number of nodes in a one-sided stencil, $N_s^o + 1$, and the number of nodes in a centred stencil, $N_s^c + 1$, are given by

$$N_s^o = I + k - 1,$$

$$N_s^c = \begin{cases} I + k - 1, & \text{if } k \text{ is odd,} \\ I + k - 2, & \text{if } k \text{ is even.} \end{cases}$$

In order to solve the eigenvalue problem it is necessary to generate the differentiation matrices $D^{(k)}$ (square matrices of size $N+1$ with elements $D_{ij}^{(k)}$) associated with the problem which approximate the derivatives of the unknown variables, i.e. which satisfy

$$h_1^{(k)} \simeq D^{(k)} \mathbf{h}_1,$$

where $\mathbf{h}_1 = (h_{1\,0}, h_{1\,1}, \ldots, h_{1\,N})^T$ in which $h_{1\,l}$ represents our approximation to $h_1(x_l)$ and k is the order of the derivative. The ith row of the matrix $D^{(k)}$ corresponds to the approximation of the kth derivative at x_i for $i = 0, \ldots, N$. The entries for the first $N_s^c/2$ rows use one-sided differences and are given by

$$D^{(k)}_{(w+1)\,(j+1)} = c^k_{j\,w}, \tag{52}$$

for $j = 0, \ldots, N_s^o$ and $w = 0, \ldots, N_s^c/2 - 1$. The entries for the next $N + 1 - N_s^c$ rows use centred differences and are given by

$$D^{(k)}_{(w+1)\,(j+w+1-N_s^c/2)} = c^k_{(j+w-N_s^c/2)\,w}, \tag{53}$$

for $j = 0, \ldots, N_s^c$ and $w = N_s^c/2, \ldots, N - N_s^c/2$. The entries for the remaining $N_s^c/2$ rows again use one-sided differences and are given by

$$D^{(k)}_{(w+1)\,(N+j+1-N_s^o)} = c^k_{(N-N_s^o+j)\,w}, \tag{54}$$

for $j = 0, \ldots, N_s^o$ and $w = N + 1 - N_s^c/2, \ldots, N$. All other elements of the matrices $D^{(k)}$ are set to zero.

The code is therefore capable of adopting arbitrary-order approximations of the derivatives appearing in the governing equation and boundary conditions. The resulting system is an algebraic eigenvalue problem of the form $A\mathbf{h_1} = \sigma B\mathbf{h_1}$, where A and B are $(N+1)$-order square matrices and σ is the corresponding eigenvalue. The system is solved by the QZ algorithm implemented using NAG routine F02GJF to determine the largest eigenvalues and (if required) the corresponding eigenvectors. In all the calculations that follow the number of grid points is set to $N = 200$ and the slip coefficient is set to $\lambda = 0.01$. The code was initially tested on several test problems with known analytical or numerical solutions and was found to give excellent agreement; again McKinley[30] gives further details. A similar numerical procedure (although an entirely different FORTRAN code) was employed by Wall and Wilson[33,34] to study the stability of certain flows of fluids with temperature-dependent viscosity.

2. Results

Figures 6(a) – (c) plot the largest eigenvalues as functions of $q \geq 0$ for $R_0 = 0.6$, 1.4 and 2.2 respectively in the case $C = 1$. Symmetric modes are denoted by solid lines and

antisymmetric modes by dashed lines. In all the numerical computations we found that only the two largest eigenvalues ever take positive values, and that one of these eigenvalues always corresponds to symmetric modes and the other always corresponds to antisymmetric modes. Typically both modes are unstable in certain ranges of q, but the nature and location of the most unstable mode (with $\sigma = \sigma^*$ at $q = q^*$) changes as R_0 is varied. When $R_0 = 0.6$ the most unstable mode is symmetric with $\sigma^* \approx 0.0171$ at $q^* \approx 1.41$ (Fig. 6(a)), but when R_0 increased to 1.4 the most unstable mode is antisymmetric with $\sigma^* \approx 0.0357$ at $q^* = 0$ (Fig. 6(b)). However, as R_0 is increased still further to 2.2 the symmetric mode once again becomes the most unstable with $\sigma^* \approx 0.0279$ at $q^* \approx 1.08$ (Fig. 6(c)). This "switching" between symmetric and antisymmetric modes as R_0 is increased is summarised in Figs. 7 and 8 which plot σ^* and q^* as functions of R_0 for a range of values of C. For completeness Fig. 7 also shows the curve for $\sigma^* = \hat{\sigma}_{s0}$ in the case $C = 0$ which is achieved in the limit $q \to 0$. Note that in both Figs. 7 and 8 there is a small region near $R_0 = 2.2$ on the curves for $C = 1$ and $C = 0.1$ that corresponds to symmetric modes, but that this region is absent from the curves for $C = 0.01$ and $C = 0.001$. Fig. 7 clearly shows that the effect of increasing C from zero is always to reduce the growth rate of the most unstable mode, and to decrease the value of R_0 at which mode switching first occurs. Figure 9 plots the largest eigenvalues when $q = 0$ as functions of R_0 for a range of values of C together with the solutions $\sigma_{a0} = JR_0^2/3$ and $\sigma_{s0} = (JR_0^3 - 6)/3R_0$ appropriate in the case $C = 0$. In particular, Fig. 9 shows how the numerically calculated values of σ when $q = 0$ approach σ_{a0} and σ_{s0} in the limit $C \to 0$.

IV. THE ANNULAR RIDGE ($0 \leq \phi_0 < 1$)

A. Basic State

Since for an annular ridge $R_2 > R_1 > 0$ Eq. (27) implies that $0 \leq \phi_0 < 1$, and so the basic-state contact angles at the "inner" and "outer" contact lines are always different. The

basic-state solution is given by Eq. (25) and the semi-volume of the ridge by Eq. (26). Figure 10 plots basic-state profiles for $R_2^0 = 2$, 2.4, 2.8 and 3.2 in the case $\phi_0 = 0.6$. These solutions are exactly the two-dimensional annular solutions described by McKinley *et al.*[6]. Note that for a given value of ϕ_0 ($0 \leq \phi_0 < 1$), solutions exist only for values of R_2^0 greater than a critical value corresponding to the limiting case in which $R_1^0 = 0$.

B. Linear Stability Problem

The governing equation for h_1 is given by Eq. (28) subject to the boundary conditions (33) and (34). Again in the special case $q = 0$ it is also necessary to impose the volume condition (37).

C. Quasi-Static Motion $C = 0$

As before, we can make considerable analytical progress in the special case of quasi-static motion ($C = 0$). Again all the analytical results presented here have been confirmed by numerical calculations.

1. Two-Dimensional Perturbations $q = 0$

From Sec. III C 1 the solution for h_1 when $C = 0$ and $q = 0$ is given by Eq. (45). Applying boundary conditions (33) and (34) and the volume condition (37) yields the expressions for the growth rates first obtained by McKinley *et al.*[6], namely $\sigma = \sigma_{+0}$ and $\sigma = \sigma_{-0}$ where

$$\sigma_{+0} = \frac{J}{12}(R_2^0 - R_1^0)^2 > 0, \tag{55}$$

$$\sigma_{-0} = \frac{J}{12}(R_2^0 - R_1^0)(R_1^0 + 3R_2^0) - \frac{4}{R_2^0 - R_1^0}. \tag{56}$$

Figure 11 plots σ_{+0} and σ_{-0} as functions of R_2^0 for $\phi_0 = 0.2$, 0.4, 0.6 and 0.8. Since $\sigma_{+0} > 0$ the ridge is always unstable when $C = 0$ and $q = 0$. Note that, unlike in the non-annular case, the analysis of McKinley *et al.*[6] includes both of the possible modes in this case.

2. Three-Dimensional Perturbations $q > 0$

From Sec. III C 2 the solution for h_1 in this case is given by Eq. (48) subject to the boundary conditions (33) and (34). Solving this system yields two expressions for σ, namely σ_+ and σ_-, given by

$$\sigma_\pm = \frac{4\zeta(12 - \zeta^2 J R_1^0)\sinh(q\zeta) - 12q\zeta^2(\phi_0 + 1)\cosh(q\zeta) \pm 3\zeta^2 X^{\frac{1}{2}}}{24\zeta^2 \sinh(q\zeta)}, \tag{57}$$

where we have written $R_2^0 = R_1^0 + \zeta$ and X is defined to be

$$X = 8q^2(\phi_0^2 + 6\phi_0 + 1) - 2J^2\zeta^2(\zeta + 2R_1^0)^2 + 2[4q^2(\phi_0 - 1)^2 + J^2\zeta^2(\zeta + 2R_1^0)^2]\cosh(2q\zeta) + 8Jq\zeta(\zeta + 2R_1^0)(\phi_0 - 1)\sinh(2q\zeta). \tag{58}$$

In particular, as $q \to 0$ we have $\sigma_\pm \to \hat{\sigma}_{\pm 0}$ where

$$\hat{\sigma}_{\pm 0} = \frac{6(3 - \phi_0) - 2JR_1^0\zeta^2 \pm 3Y^{\frac{1}{2}}}{12\zeta}, \tag{59}$$

where Y is defined to be

$$Y = 4(1 + \phi_0)^2 + 4J\zeta^2(\zeta + 2R_1^0)(\phi_0 - 1) + J^2\zeta^4(\zeta + 2R_1^0)^2. \tag{60}$$

Note that $\hat{\sigma}_{+0} \neq \sigma_{+0}$ and $\hat{\sigma}_{-0} \neq \sigma_{-0}$, i.e. because neither of these solutions satisfy the volume condition (37) for $q > 0$ we do not recover the expressions obtained previously in the case $q = 0$ in the limit $q \to 0$. The neutral stability curves for $q > 0$ obtained by setting $\sigma_+ = 0$ in Eq. (57) are plotted in Fig. 12 for $\phi_0 = 0.2$, 0.4, 0.6 and 0.8. In particular, Fig. 12 shows that the region of instability widens as ϕ_0 is increased from zero.

Figure 13 plots the growth rates σ_+ and σ_- as functions of $q \geq 0$ for $R_2^0 = 2.5$, 3, 3.5 and 4 for $\phi_0 = 0.2$. Note that the filled circles at $q = 0$ correspond to $\sigma_{\pm 0}$, i.e. to the modes obtained by McKinley *et al.*[6]. Since $\sigma_+ > \sigma_-$ for $q > 0$, both σ_+ and σ_- are monotonically decreasing functions of q for all $q > 0$, $\hat{\sigma}_{+0} > \sigma_{+0} > \hat{\sigma}_{-0} > \sigma_{-0}$ and $\hat{\sigma}_{+0} > 0$, we deduce that the long-wavelength modes with growth rate approaching $\hat{\sigma}_{+0}$ in the limit $q \to 0$ are always the most unstable when $C = 0$.

D. The General Case $C \neq 0$

The neutral stability curves when $C \neq 0$ (obtained by setting $\sigma = 0$ in Eqs (28), (33) and (34)) are the same as those calculated previously in the case $C = 0$ and shown in Fig. 12. Again, when $\sigma \neq 0$ we must proceed numerically.

Figure 14 plots the largest eigenvalues as functions of $q \geq 0$ for $R_2^0 = 2.5$, 3, 3.5 and 4 for $\phi_0 = 0.2$ in the case $C = 1$. As Fig. 14 shows, as R_0 is increased the values of $\sigma^* > 0$ and q^* increase and so the ridge is again unconditionally unstable. However, the switching between modes seen in the non-annular case does not occur in this case. This behaviour is summarised in Figs. 15 and 16 which plot σ^* and q^* as functions of R_2^0 for a range of values of C. For completeness Fig. 15 also shows the curve for $\sigma^* = \hat{\sigma}_{+0}$ in the case $C = 0$ which is achieved when $q = 0$. Fig. 15 clearly shows that, as in the non-annular case, the effect of increasing C from zero is always to reduce the growth rate of the most unstable mode. Figure 17 plots the largest eigenvalues when $q = 0$ as functions of R_2^0 for a range of values of C together with the solutions σ_{+0} and σ_{-0} appropriate in the case $C = 0$. In particular, Fig. 17 shows how the numerically calculated values of σ when $q = 0$ approach σ_{+0} and σ_{-0} in the limit $C \to 0$.

V. CONCLUSIONS

In this paper we investigated the linear stability of an initially symmetric two-dimensional thin ridge of Newtonian fluid of finite width on a horizontal planar substrate acting under the influence of a jet of air normal to the substrate. Both annular and non-annular ridges were considered. For both problems we examined both the special case of quasi-static motion (corresponding to zero capillary number) analytically and the general case of non-zero capillary number numerically. In all cases the ridge was found to be unconditionally unstable, but the nature and location of the most unstable mode were found to depend on the details of the specific problem considered.

For a non-annular ridge we found that for two-dimensional quasi-static motion the conditionally stable symmetric mode described by McKinley *et al.*[6] is always more stable than the unconditionally unstable antisymmetric mode. For general quasi-static motion the ridge is always most unstable to a long-wavelength symmetric mode. When $C \neq 0$ the growth rate of the most unstable mode is reduced relative to the case $C = 0$ and the nature and location of the most unstable mode switches between long-wavelength and finite-wavelength modes as R_0 is varied.

A similar analysis was performed for an annular ridge. For two-dimensional quasi-static motion we recovered the results of McKinley *et al.*[6], while for general quasi-static motion the ridge is always unstable to a long-wavelength mode. When $C \neq 0$ the growth rate of the most unstable mode is again reduced relative to the case $C = 0$, the ridge is always most unstable to a mode with finite wavelength and the switching between different types of modes and values of q found in the non-annular case does not occur.

The basic destabilising effect of the air jet can be understood physically as follows. When $C = 0$ the pressure within the ridge is spatially uniform and the quasi-static shapes of both annular and non-annular ridges are determined by a balance between capillary forces (which tend to minimise the surface area of the ridge) and the force due to the air jet, with the result that the effect of the air jet is always to tend to increase the contact angle at an advancing contact line and to decrease it at a retreating one. However, the forms of the Tanner laws mean that these situations are self-reinforcing and so the effect of the air jet is always a destabilising one. It should, however, be emphasised that even in the absence of the air jet, the interplay between capillary forces and the Tanner laws can be sufficient to make the non-annular ridge unstable. (An annular ridge cannot occur in the absence of the air jet.) Specifically, while all anti-symmetric and sufficiently short-wavelength symmetric transverse perturbations decrease the contact angle at an advancing contact line and increase the contact angle at a retreating contact line and are therefore stable, sufficiently long-wavelength symmetric transverse perturbations have the opposite effect and are therefore unstable. Thus modes that are unstable in the absence of the air jet become more unstable

in its presence, while modes that are stable in the absence of the air jet become less stable and can be made unstable for sufficiently large J (i.e. for sufficiently strong jets, large ridges, small surface tension or small static contact angle). In the case $C = 0$ the bulk of the ridge instantaneously adopts a quasi-static shape whose subsequent motion is entirely determined by the motion of the contact lines on a timescale of L/κ. When $C \neq 0$ the bulk of the ridge responds on a timescale of $\mu L/\tau\theta_0^3$ (which differs from the contact-line timescale by a factor of C) and so the motion is always retarded relative to the case $C = 0$.

Natural extensions of the present work would be to investigate the effect of gravity on the above results and, perhaps more interestingly, to tackle the initially asymmetric version of the present two-dimensional problem or the corresponding initially axisymmetric three-dimensional problem. It would, of course, also be of considerable interest to compare the predictions of the present theoretical calculations with experimental results.

ACKNOWLEDGEMENTS

During the course of the present work the first author (ISM) was supported by the University of Strathclyde, Glasgow, Scotland, UK, via the Graduate Teaching Assistant Scheme. This work was begun while the second author (SKW) was a Visiting Scholar in the Department of Engineering Science and Applied Mathematics of Northwestern University, Evanston, IL, where he was partly supported under a United States Department of Energy Grant in the Basic Energy Sciences while he was visiting Professor S. G. Bankoff and Professor S. H. Davis. Both authors wish to thank both Professor D. M. Sloan and Dr. B. R. Duffy (Department of Mathematics, University of Strathclyde) for invaluable discussions during the course of the present work.

REFERENCES

[1] A. Oron, S. H. Davis and S. G. Bankoff, "Long-scale evolution of thin liquid films," Rev. Mod. Phys **69** 931 (1997).

[2] T. G. Myers, "Thin films with high surface tension," SIAM Rev. **40** 441 (1998).

[3] J. A. Moriarty, L. W. Schwartz and E. O. Tuck, "Unsteady spreading of thin liquid films with small surface tension," Phys. Fluids A **3**, 733 (1991).

[4] A. C. King, E. O. Tuck and J. -M. Vanden-Broeck, "Air-blown waves on thin viscous sheets," Phys. Fluids A **5**, 973 (1993).

[5] A. C. King and E. O. Tuck, "Thin liquid layers supported by steady air-flow surface traction," J. Fluid Mech. **251**, 709 (1993).

[6] I. S. McKinley, S. K. Wilson and B. R. Duffy, "Spin coating and air-jet blowing of thin viscous drops," Phys. Fluids. **11**, 30 (1999).

[7] J. A. Thornton and H. F. Graff, "An analytical description of the jet finishing process for hot-dip metallic coatings on strip," Metallurgical Trans. B **7B** 607 (1976).

[8] E. O. Tuck, "Continuous coating with gravity and jet stripping," Phys. Fluids **26**, 2352 (1983).

[9] C. H. Ellen and C. V. Tu, "An analysis of jet stripping of liquid coatings," J. Fluids Eng. **106**, 399 (1984).

[10] E. O. Tuck and J. -M. Vanden-Broeck, "Influence of surface tension on jet-stripped continuous coating of sheet materials," A. I. Ch. E. Journal **30**, 808 (1984).

[11] J. J. Kriegsmann, M. J. Miksis and J. -M. Vanden-Broeck, "Pressure driven disturbances on a thin viscous film," Phys. Fluids **10**, 1249 (1998).

[12] S. M. Troian, E. Herbolzheimer, S. A. Safran and J. F. Joanny, "Fingering instabilities of driven spreading films," Europhys. Lett. **10**, 25 (1989).

[13] M. A. Spaid and G. M. Homsy, "Stability of Newtonian and viscoelastic dynamic contact lines," Phys. Fluids **8**, 460 (1996).

[14] A. L. Bertozzi and M. P. Brenner, "Linear stability and transient growth in driven contact lines," Phys. Fluids **9**, 530 (1997).

[15] P. G. López, S. G. Bankoff and M. J. Miksis, "Non-isothermal spreading of a thin liquid film on an inclined plane," J. Fluid Mech. **324**, 261 (1996).

[16] P. G. López, M. J. Miksis and S. G. Bankoff, "Inertial effects on contact line instability in the coating of a dry inclined plate," Phys. Fluids **9**, 2177 (1997).

[17] D. E. Kataoka and S. M. Troian, "A theoretical study of instabilities at the advancing front of thermally driven coating films," J. Coll. Int. Sci. **192**, 350 (1997).

[18] D. E. Kataoka and S. M. Troian, "Stabilizing the advancing front of thermally driven climbing films," J. Coll. Int. Sci. **203**, 335 (1998).

[19] L. M. Hocking, "Spreading and instability of a viscous fluid sheet," J. Fluid Mech. **211**, 373 (1990).

[20] L. M. Hocking and M. J. Miksis, "Stability of a ridge of fluid," J. Fluid Mech. **247**, 157 (1993).

[21] J. A. Moriarty and L. W. Schwartz, "Dynamic considerations in the closing and opening of holes in thin liquid films," J. Coll. Int. Sci. **161**, 335 (1993).

[22] S. K. Wilson and E. L. Terrill, "The dynamics of planar and axisymmetric holes in thin fluid layers," in *First European Coating Symposium on the Mechanics of Thin Film Coatings, Leeds University, UK, 19-22 September 1995*, (eds. P. H. Gaskell, M. D. Savage and J. L. Summers), World Scientific, Singapore, 1996. pp. 288.

[23] P. G. López, M. J. Miksis and S. G. Bankoff, "Stability and evolution of a dry spot," Northwestern University Applied Mathematics Technical Report 9605 (July 1997).

[24] H. P. Greenspan, "On the motion of a small viscous droplet that wets a surface," J. Fluid Mech. **84**, 125 (1978).

[25] P. Ehrhard and S. H. Davis, "Non-isothermal spreading of liquid drops on horizontal plates," J. Fluid Mech. **229**, 365 (1991).

[26] D. M. Anderson and S. H. Davis. "The spreading of volatile droplets on heated surfaces," Phys. Fluids **7**, 248 (1995).

[27] L. M. Hocking, "Rival contact-angle models and the spreading of drops," J. Fluid Mech. **239**, 671 (1992).

[28] L. M. Hocking, "On contact angles in evaporating liquids," Phys. Fluids **7**, 2950 (1995).

[29] P. J. Haley and M. J. Miksis, "The effect of the contact line on droplet spreading," J. Fluid Mech. **223**, 57 (1991).

[30] I. S. McKinley, "Studies in thin-film flows," Ph. D. Thesis, University of Strathclyde, Glasgow, United Kingdom, July 1999.

[31] M. Vinokur, "On one-dimensional stretching functions for finite-difference calculations," J. Comp. Phys. **50**, 215 (1983).

[32] B. Fornberg, "Calculation of weights in finite difference formulas," SIAM Rev. **40**, 685 (1998).

[33] D. P. Wall and S. K. Wilson, "The linear stability of channel flow of fluid with temperature-dependent viscosity," J. Fluid Mech. **323**, 107 (1996).

[34] D. P. Wall and S. K. Wilson, "The linear stability of flat-plate boundary-layer flow of fluid with temperature-dependent viscosity," Phys. Fluids **9**, 2885 (1997).

FIGURES

FIG. 1. Geometry of the non-annular problem.

FIG. 2. Basic-state profiles of the non-annular ridge for $R_0 = 0.6$, 1, 1.4, 1.8 and 2.2.

FIG. 3. Plot of the growth rates of symmetric (σ_{s0}) and antisymmetric (σ_{a0}) modes as functions of R_0 for the non-annular ridge in the case $q = 0$ and $C = 0$.

FIG. 4. Neutral stability curves for symmetric ($\sigma_s = 0$) and antisymmetric ($\sigma_a = 0$) modes in the (q,R_0) plane for the non-annular ridge in the case $q > 0$ and $C = 0$. Here (S) denotes symmetric modes and (A) antisymmetric modes.

FIG. 5. (a) – (b): Plot of the growth rates of symmetric (σ_s) and antisymmetric (σ_a) modes as functions of $q \geq 0$ for the non-annular ridge for $R_0 = 1$ and 2.2 respectively in the case $C = 0$. Symmetric modes are denoted by solid lines and antisymmetric modes by dashed lines. At $q = 0$, a filled circle denotes a solution, an empty circle no solution.

FIG. 6. (a) – (c): Plot of the largest eigenvalues as functions of $q \geq 0$ for the non-annular ridge for $R_0 = 0.6$, 1.4 and 2.2 respectively in the case $C = 1$. Symmetric modes are denoted by solid lines and antisymmetric modes by dashed lines. At $q = 0$, a filled circle denotes a solution, an empty circle no solution.

FIG. 7. Plot of σ^* as a function of R_0 for the non-annular ridge for $C = 1$, 0.1, 0.01, 0.001 and $C = 0$. Symmetric modes are denoted by solid lines and antisymmetric modes by dashed lines.

FIG. 8. Plot of q^* as a function of R_0 for the non-annular ridge for $C = 1$, 0.1, 0.01 and 0.001. Symmetric modes are denoted by solid lines and antisymmetric modes by dashed lines.

FIG. 9. Plot of the largest eigenvalues when $q = 0$ as functions of R_0 for the non-annular ridge for $C = 1$, 0.1, 0.01 and 0.001. Symmetric modes are denoted by solid lines and antisymmetric modes by dashed lines. The thin curves denote the eigenvalues obtained numerically when $C \neq 0$ and the thick curves denote the solutions $\sigma_{s0} = (JR_0^3 - 6)/3R_0$ and $\sigma_{a0} = JR_0^2/3$ appropriate in the case $C = 0$.

FIG. 10. Basic-state profiles of the annular ridge for $R_2^0 = 2$, 2.4, 2.8 and 3.2 in the case $\phi_0 = 0.6$.

FIG. 11. Plot of the growth rates σ_{+0} and σ_{-0} as functions of R_2^0 for the annular ridge for $\phi_0 = 0.2$, 0.4, 0.6 and 0.8 in the case $q = 0$ and $C = 0$.

FIG. 12. Neutral stability curves in the (q,R_2^0) plane corresponding to $\sigma_+ = 0$ for the annular ridge for $\phi_0 = 0.2$, 0.4, 0.6 and 0.8 in the case $q > 0$ and $C = 0$.

FIG. 13. Plot of the growth rates σ_+ and σ_- as functions of $q \geq 0$ for the annular ridge for $R_2^0 = 2.5$, 3, 3.5 and 4 for $\phi_0 = 0.2$ in the case $C = 0$. At $q = 0$, a filled circle denotes a solution, an empty circle no solution.

FIG. 14. Plot of the largest eigenvalues as functions of $q \geq 0$ for the annular ridge for $R_2^0 = 2.5$, 3, 3.5 and 4 for $\phi_0 = 0.2$ in the case $C = 1$. At $q = 0$, a filled circle denotes a solution, an empty circle no solution.

FIG. 15. Plot of σ^* as a function of R_2^0 for the annular ridge for $C = 1$, 0.1, 0.01, 0.001 and $C = 0$ in the case $\phi_0 = 0.6$.

FIG. 16. Plot of q^* as a function of R_2^0 for the annular ridge for $C = 1$, 0.1, 0.01 and 0.001 in the case $\phi_0 = 0.6$.

FIG. 17. Plot of the largest eigenvalues when $q = 0$ as functions of R_2^0 for the annular ridge for $C = 1$, 0.1, 0.01 and 0.001 in the case $\phi_0 = 0.6$. The thin curves denote the eigenvalues obtained numerically when $C \neq 0$ and the thick curves denote the eigenvalues $\sigma_{\pm 0}$ appropriate in the case $C = 0$.

McKinley, Phys. Fluids

Fig. 1

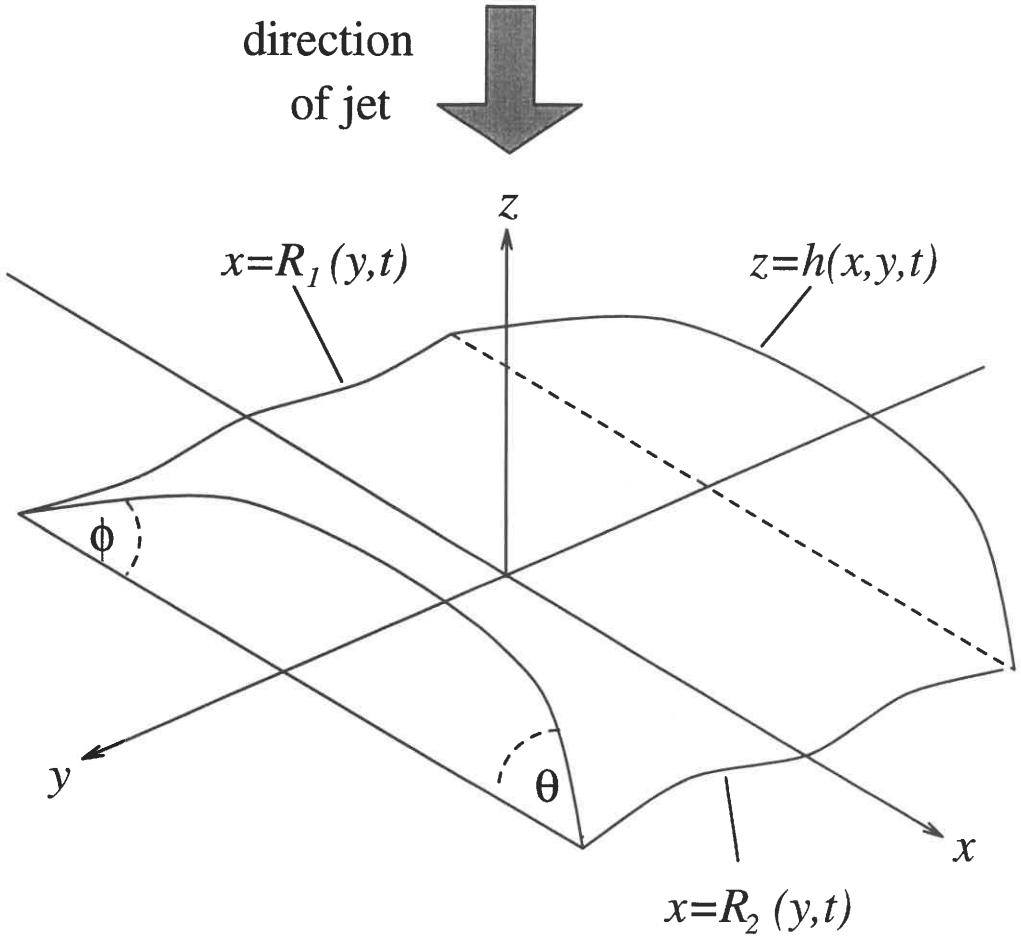

McKinley, Phys. Fluids

Fig. 2

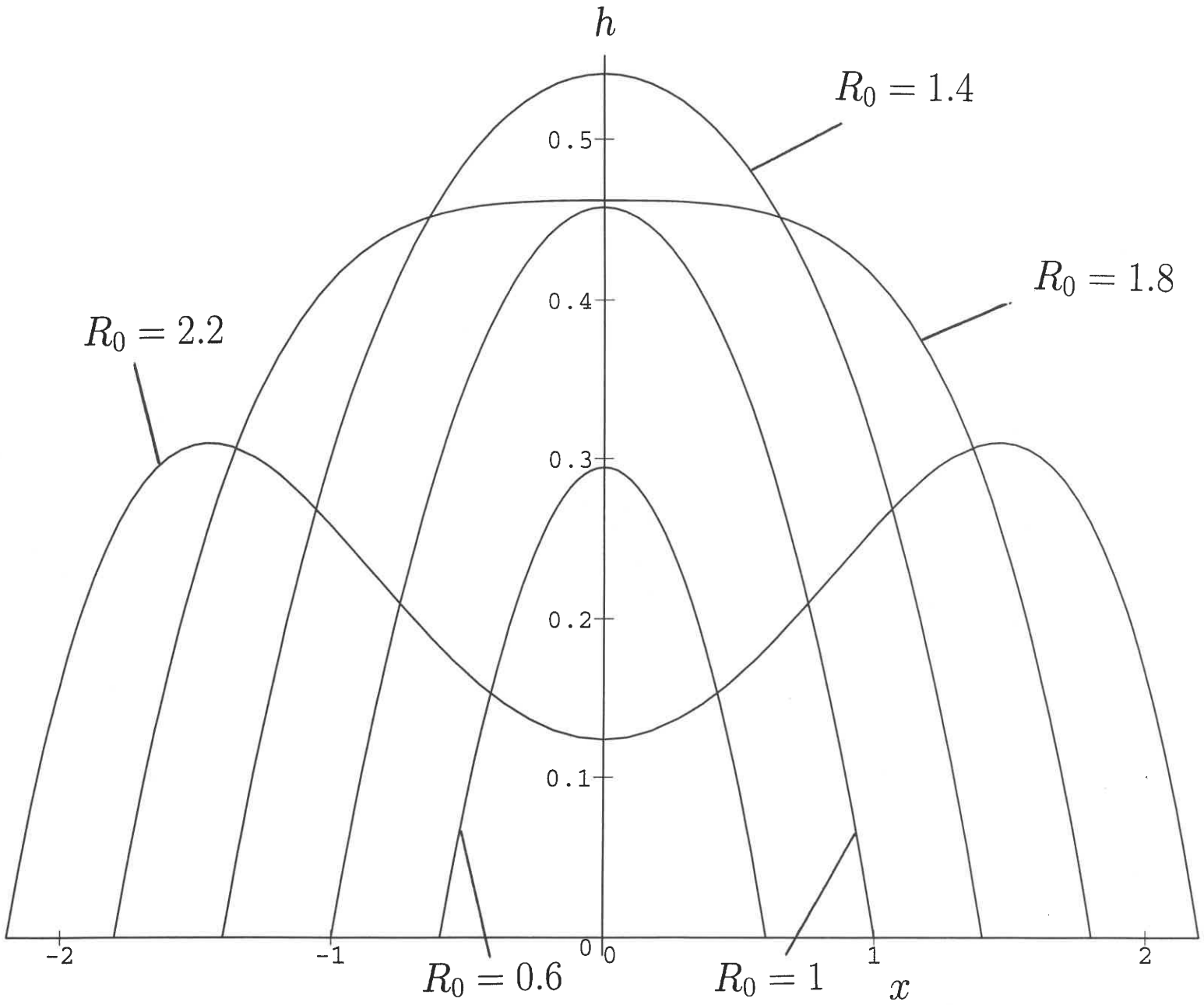

McKinley, Phys. Fluids

Fig. 3

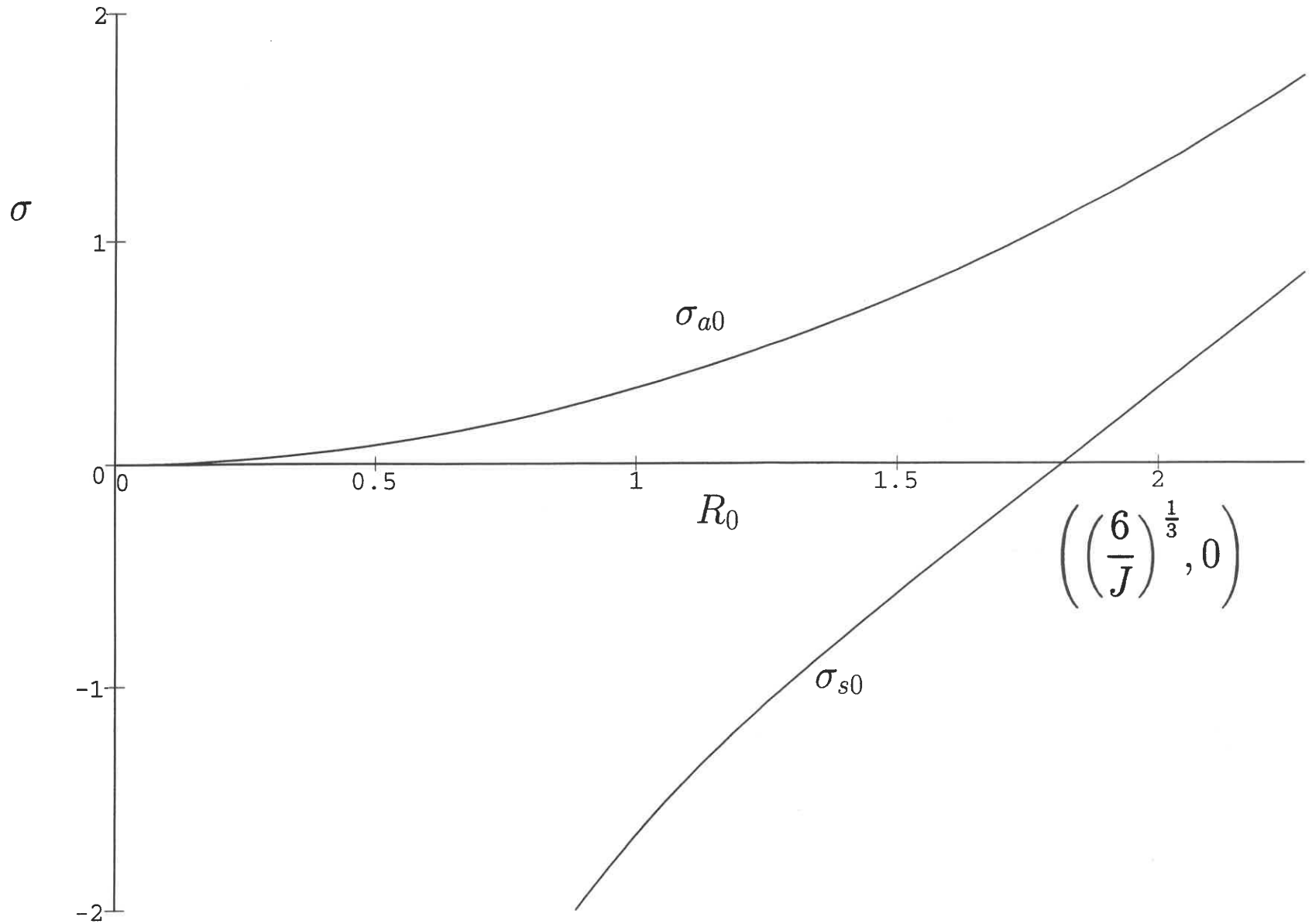

McKinley, Phys. Fluids

Fig. 4

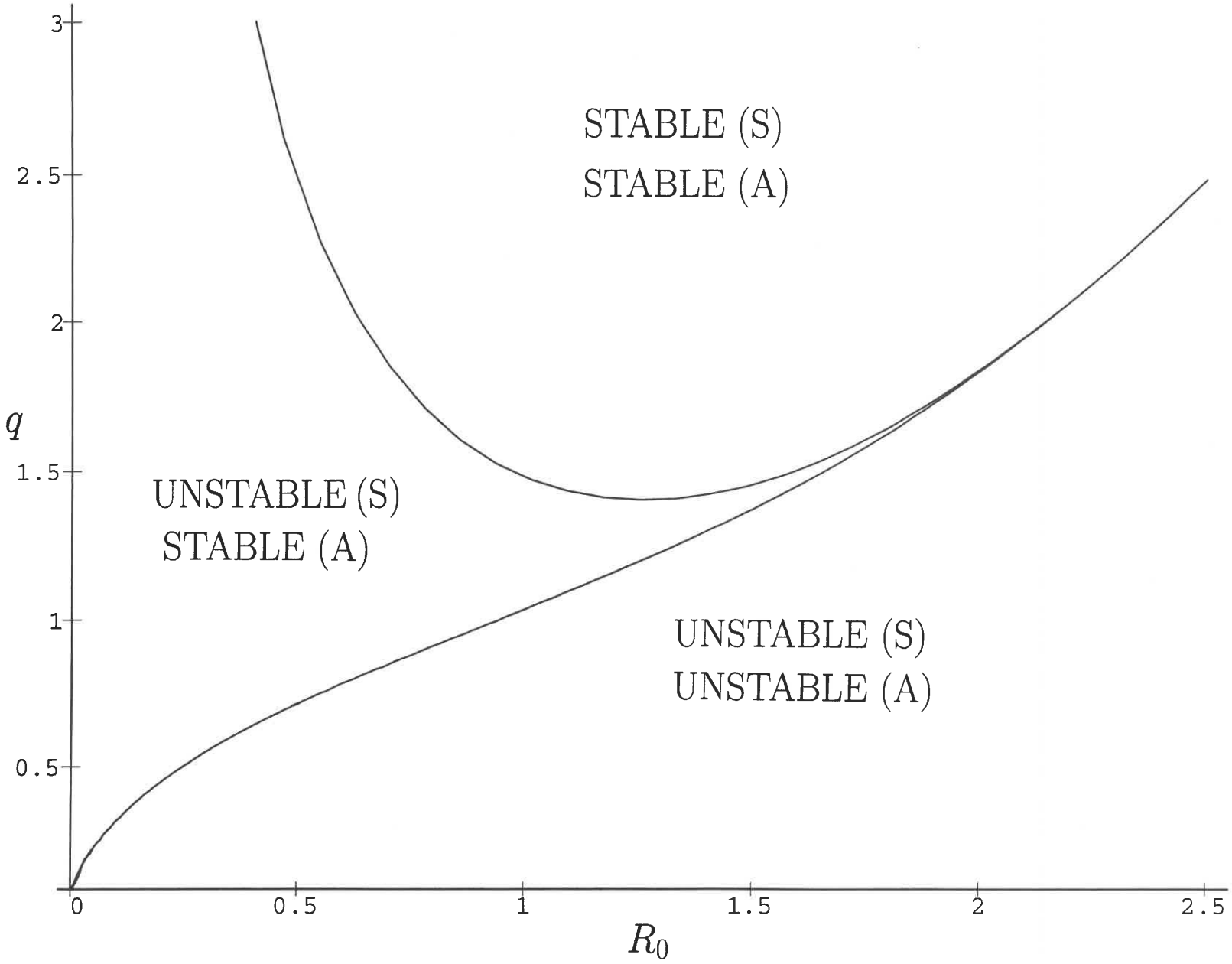

McKinley, Phys. Fluids Fig. 5(a)

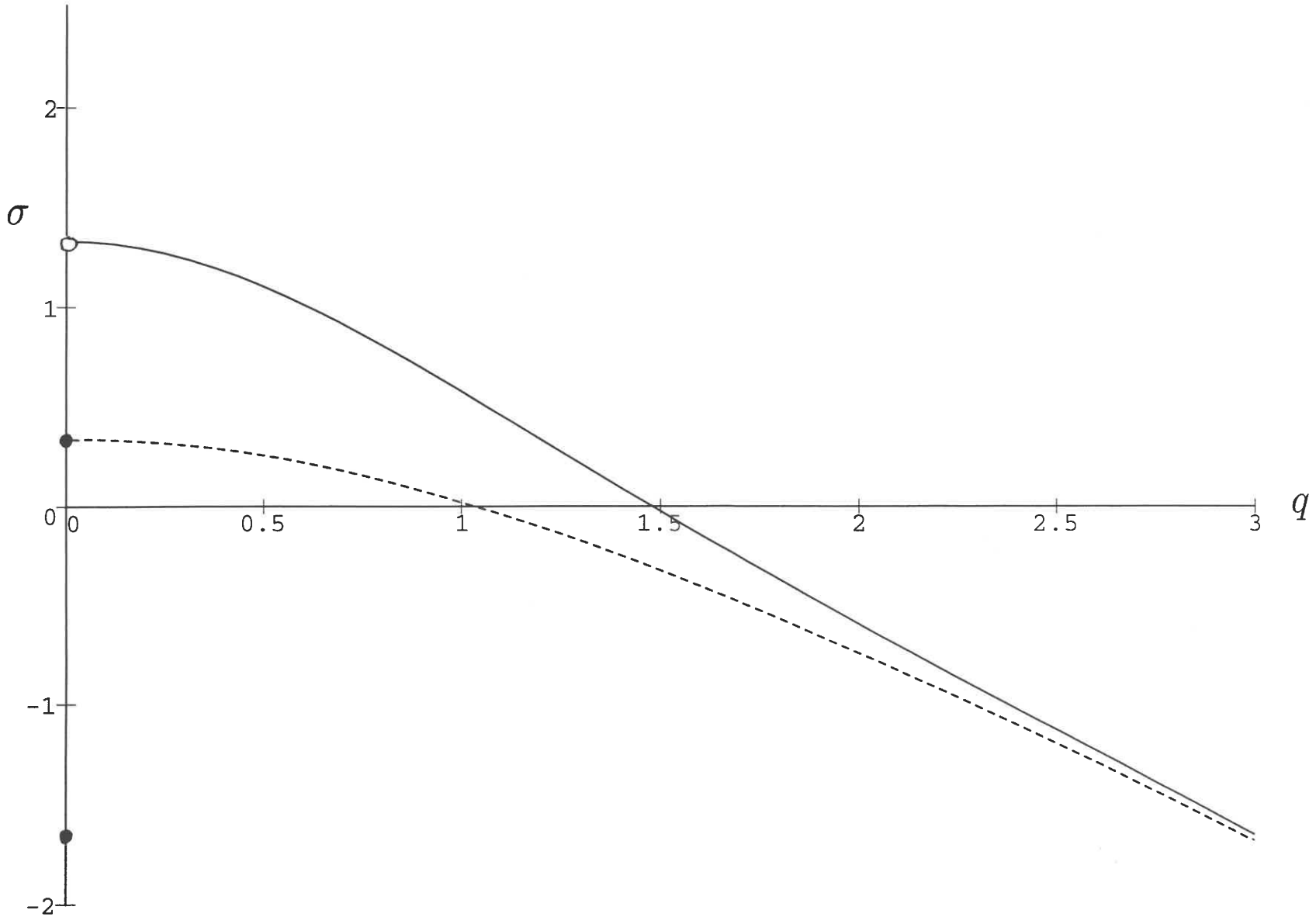

McKinley, Phys. Fluids

Fig. 5(b)

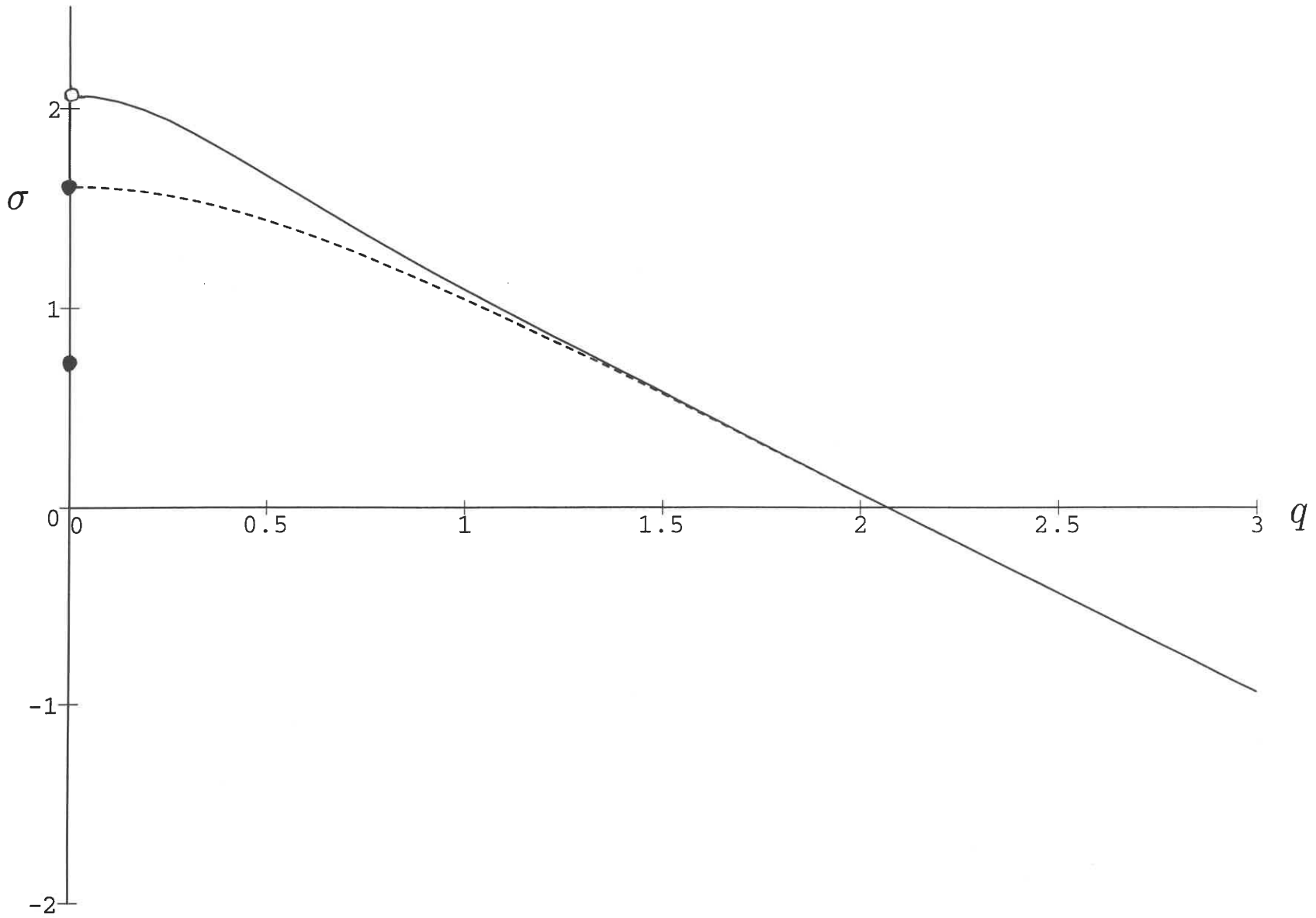

McKinley, Phys. Fluids

Fig. 6(a)

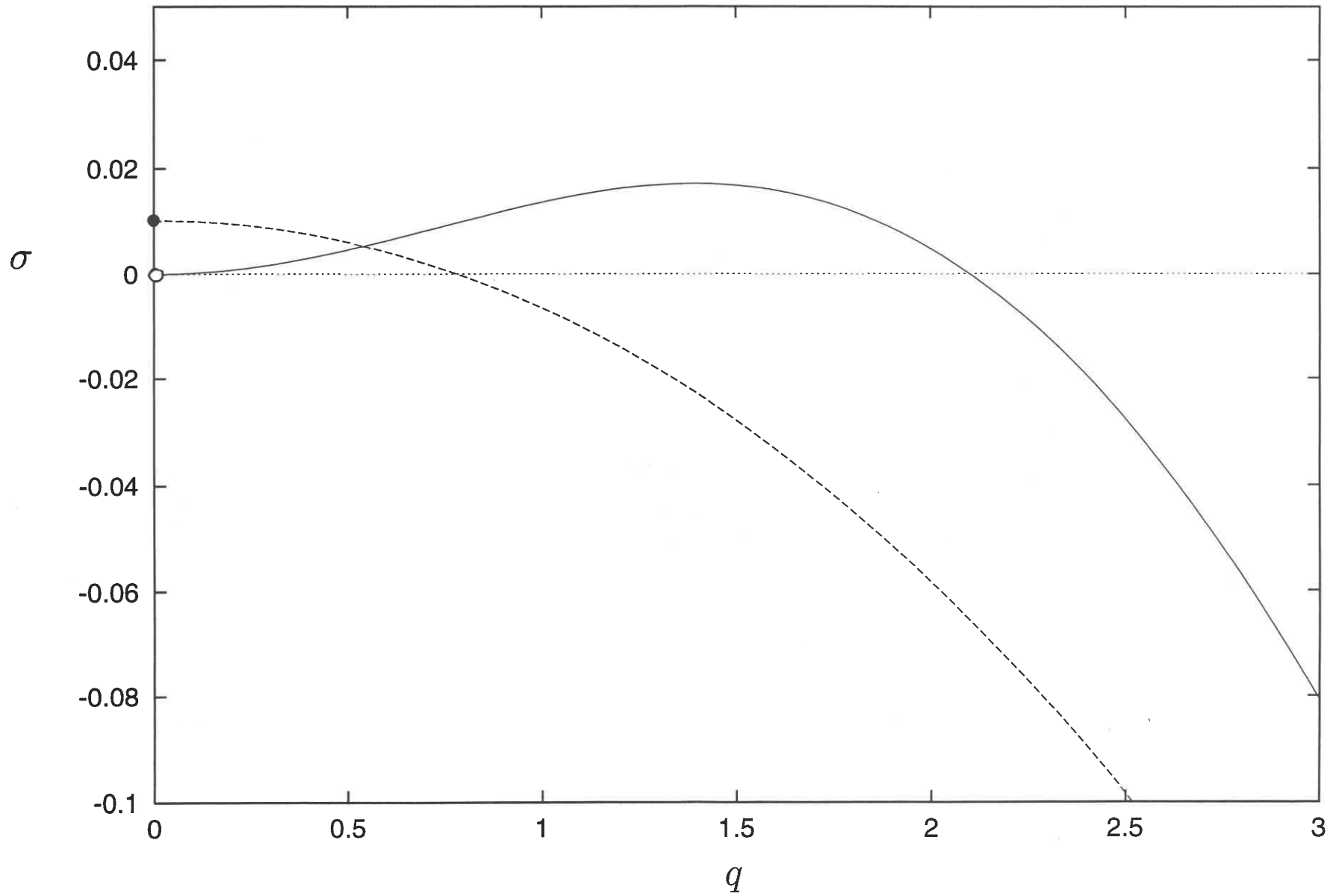

McKinley, Phys. Fluids

Fig. 6(b)

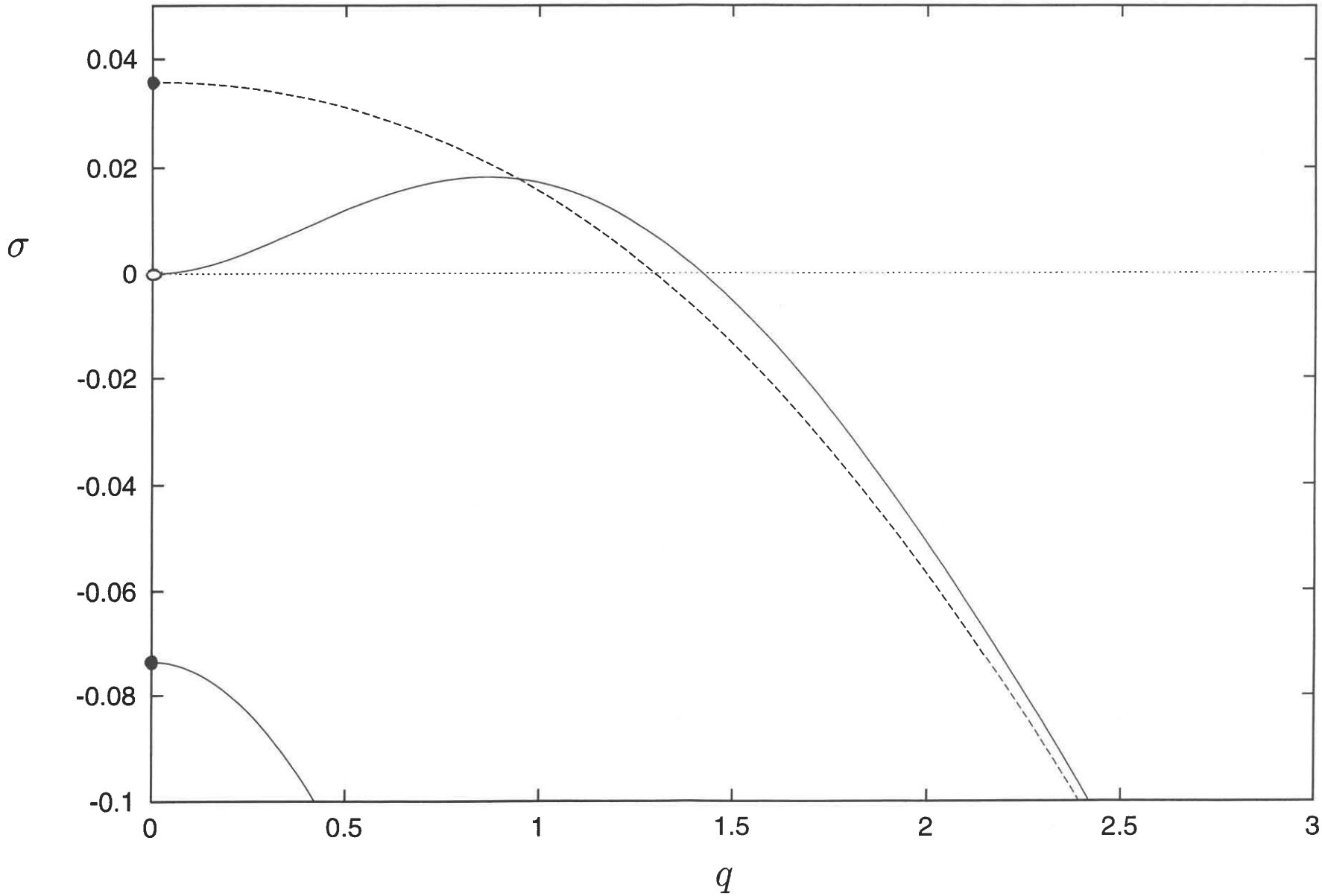

McKinley, Phys. Fluids Fig. 6(c)

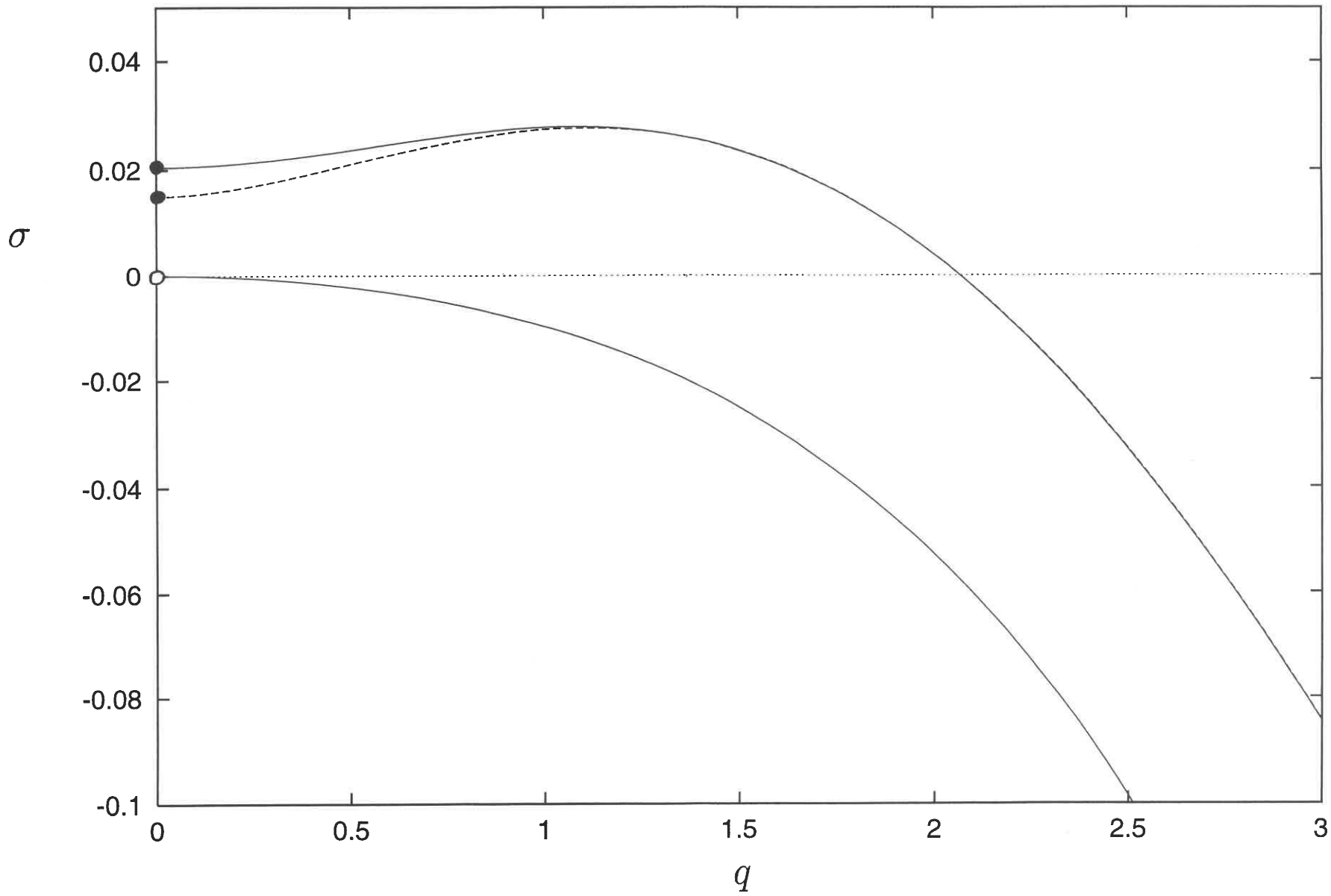

McKinley, Phys. Fluids Fig. 7

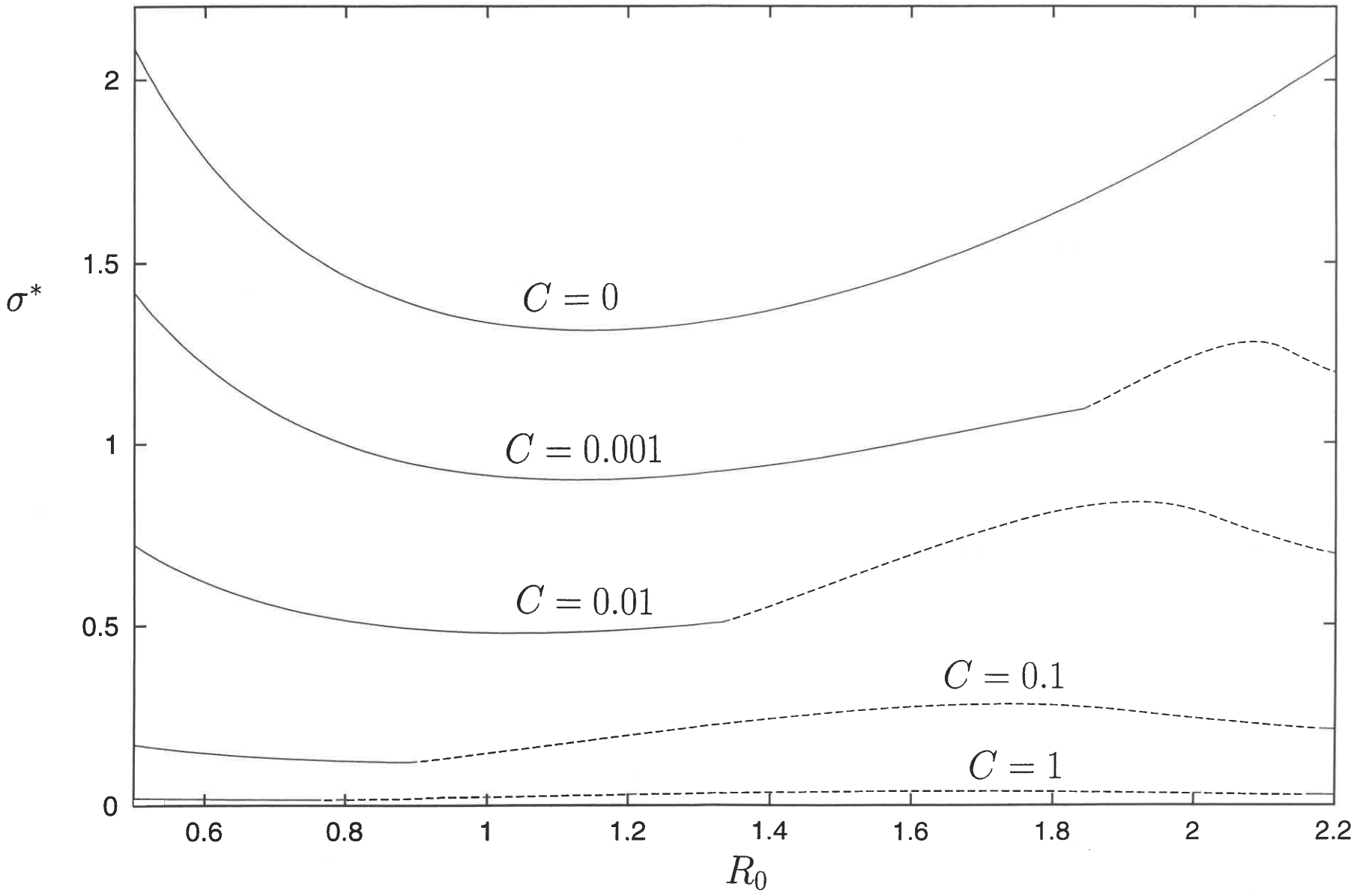

McKinley, Phys. Fluids Fig. 8

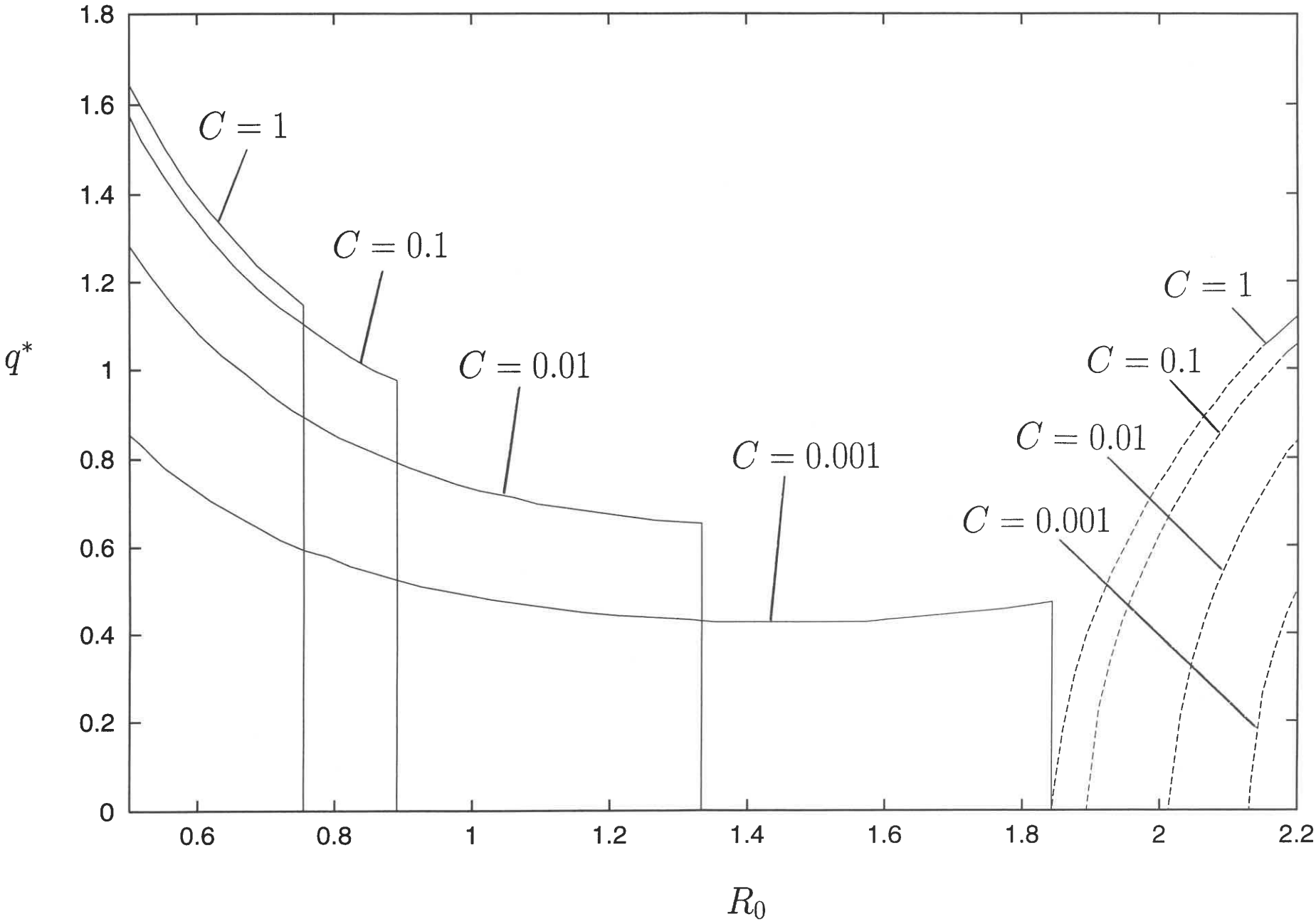

McKinley, Phys. Fluids Fig. 9

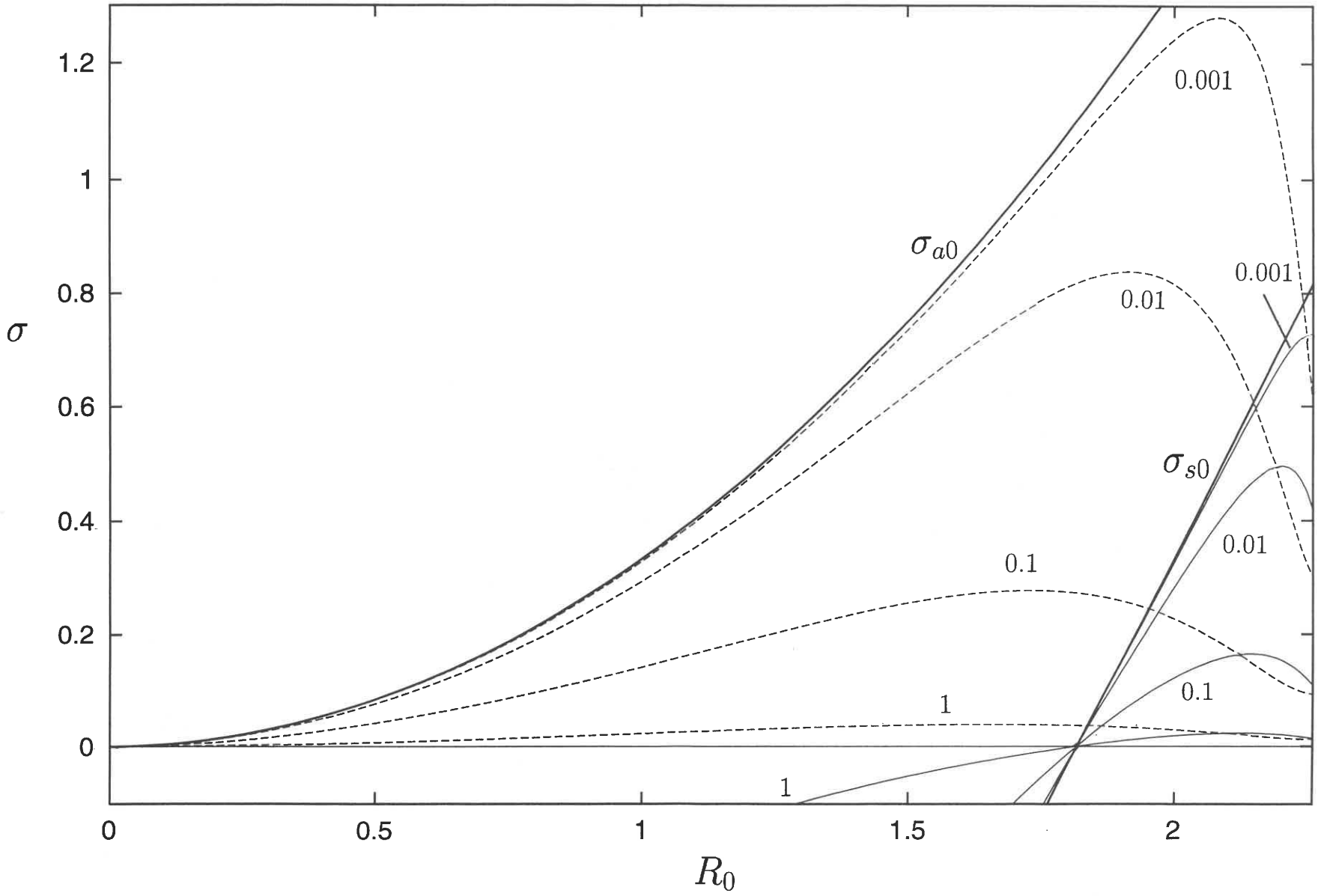

McKinley, Phys. Fluids

Fig. 10

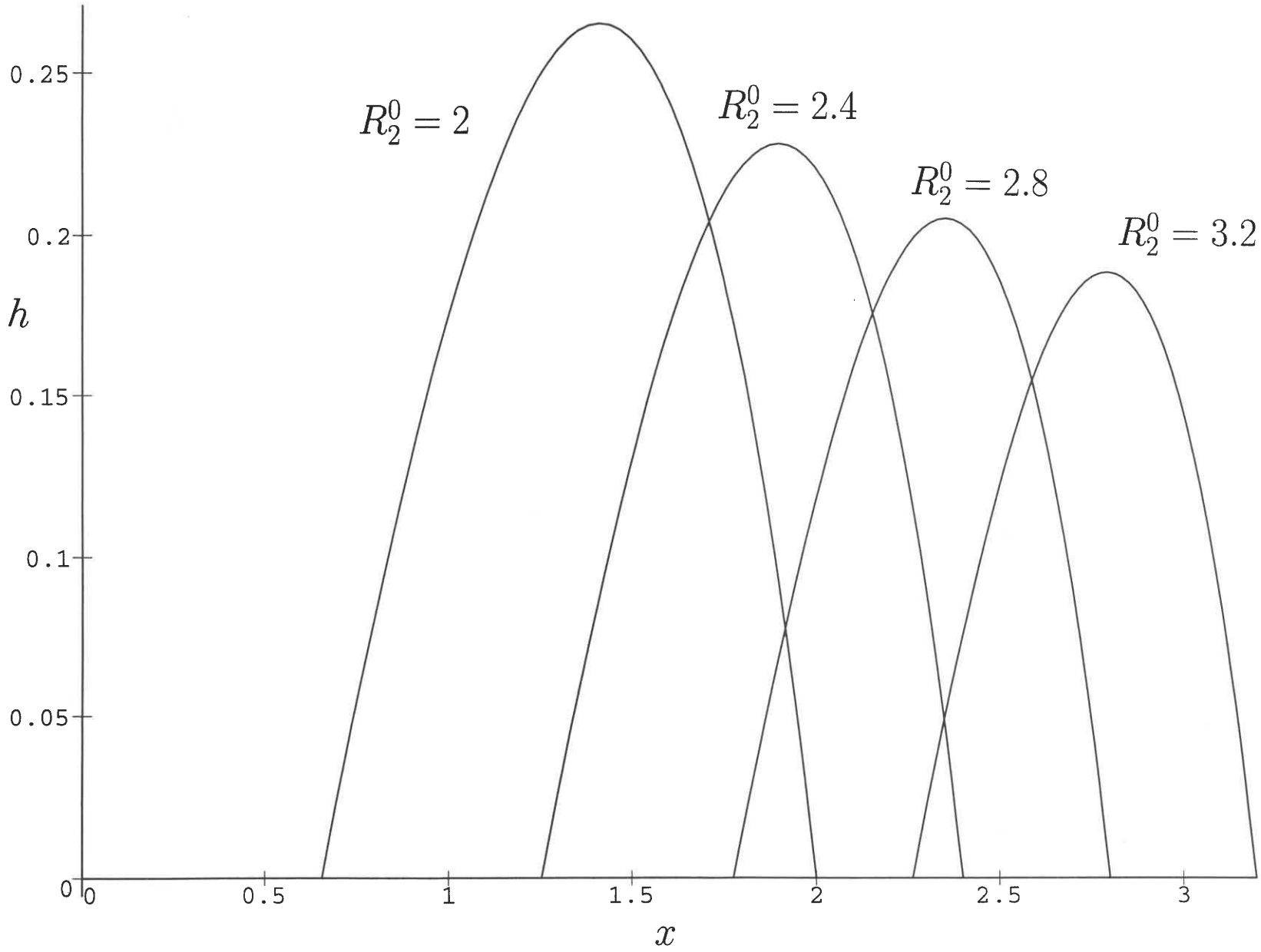

McKinley, Phys. Fluids

Fig. 11

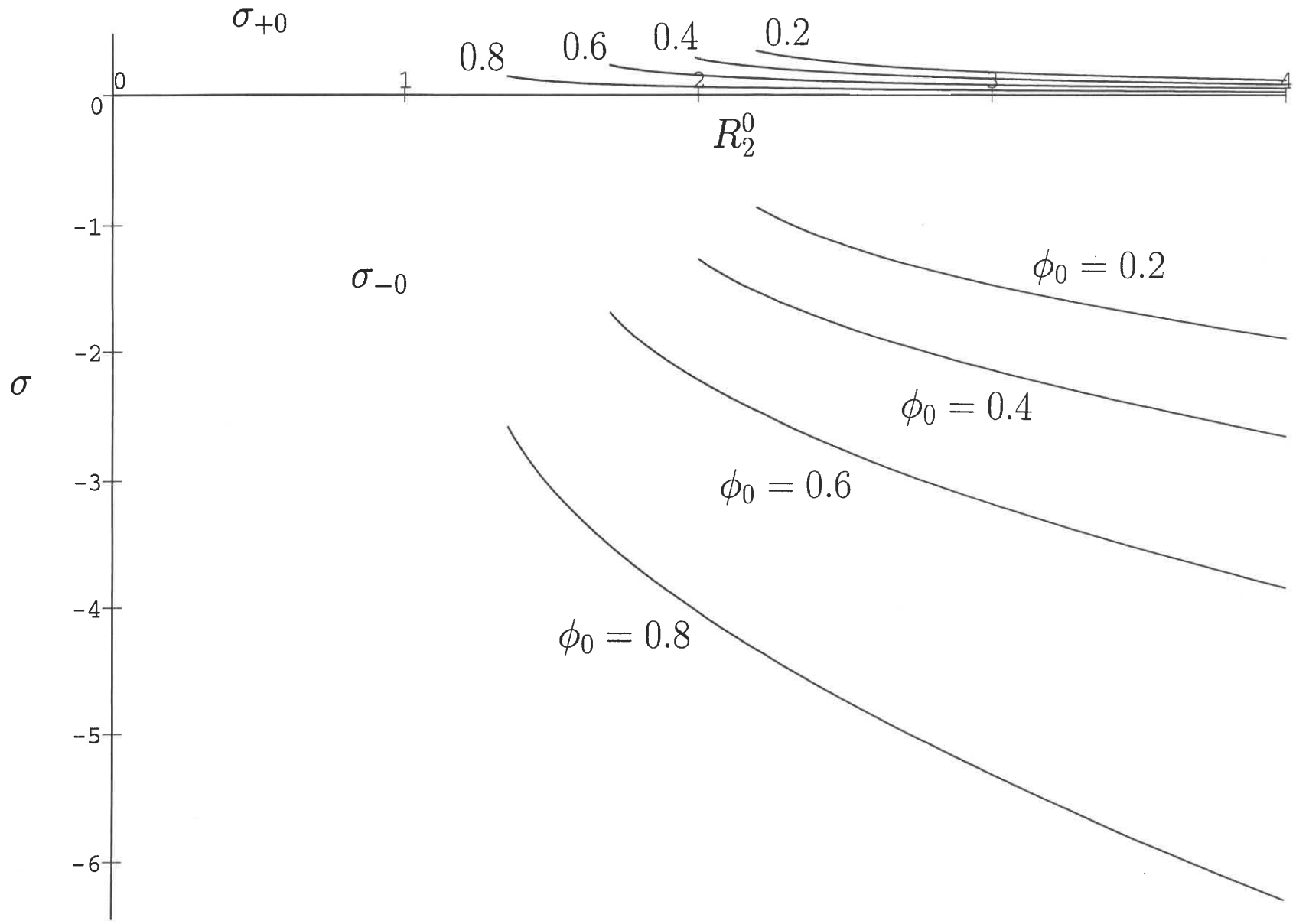

McKinley, Phys. Fluids Fig. 12

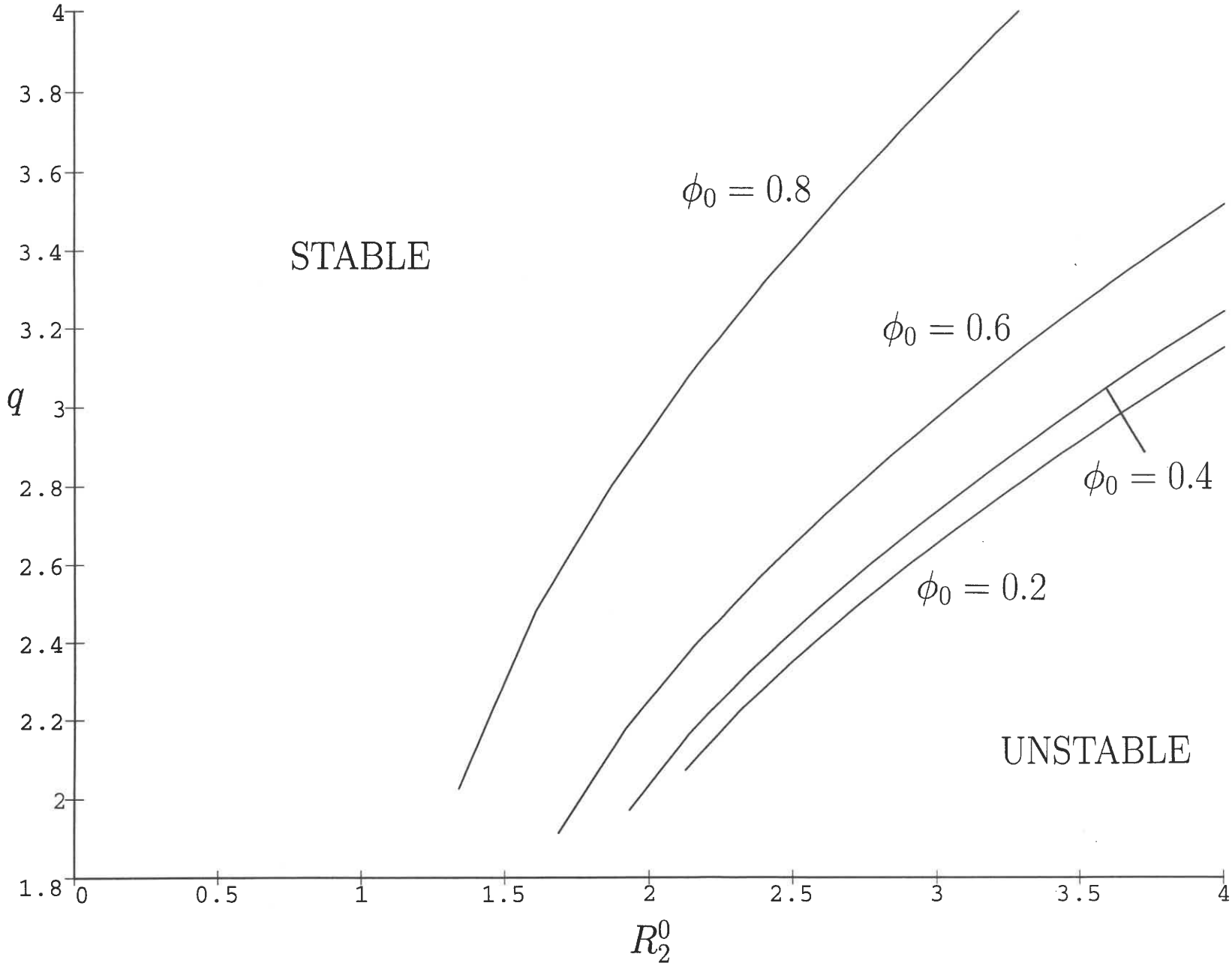

McKinley, Phys. Fluids Fig. 13

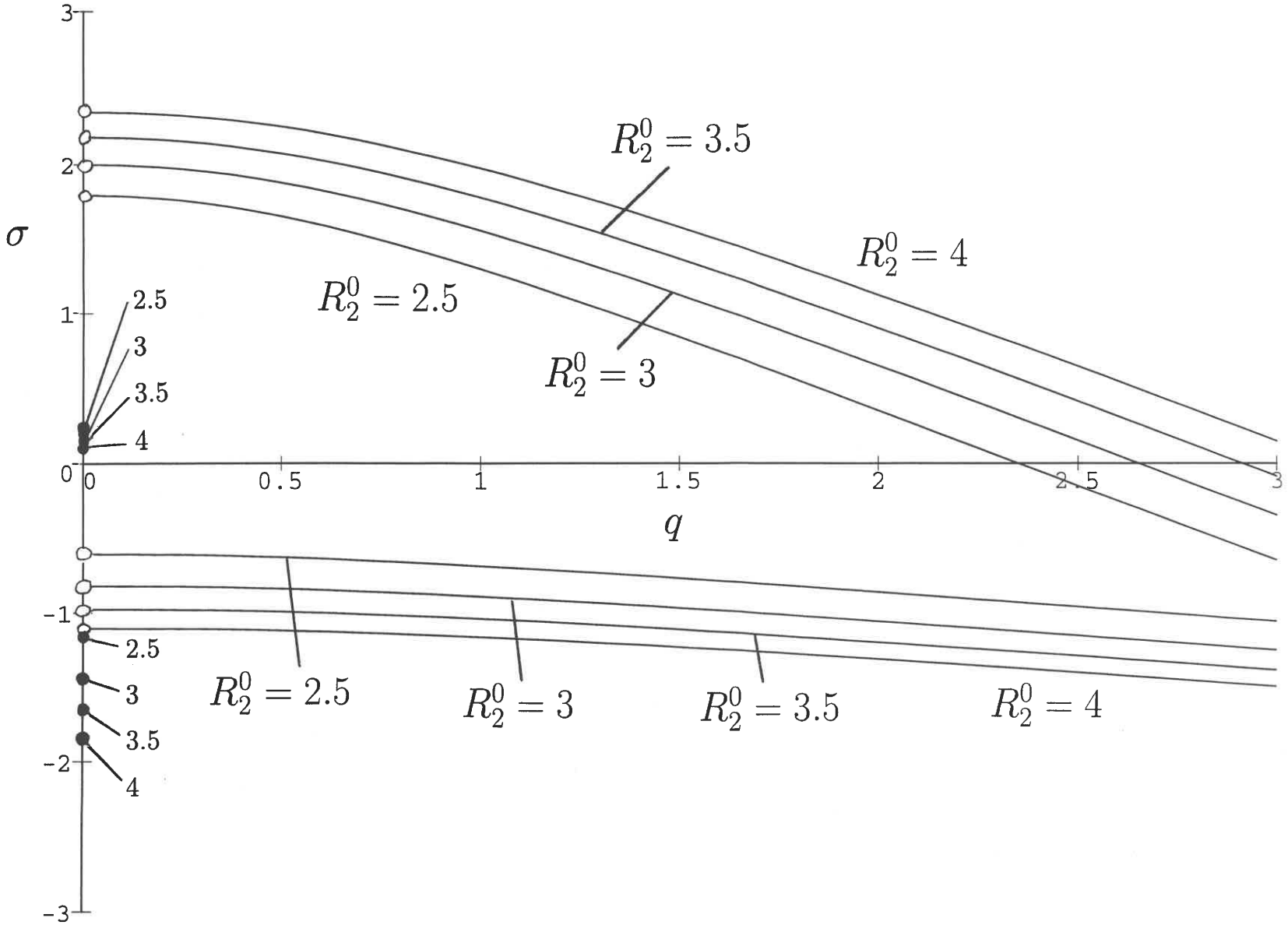

McKinley, Phys. Fluids

Fig. 14

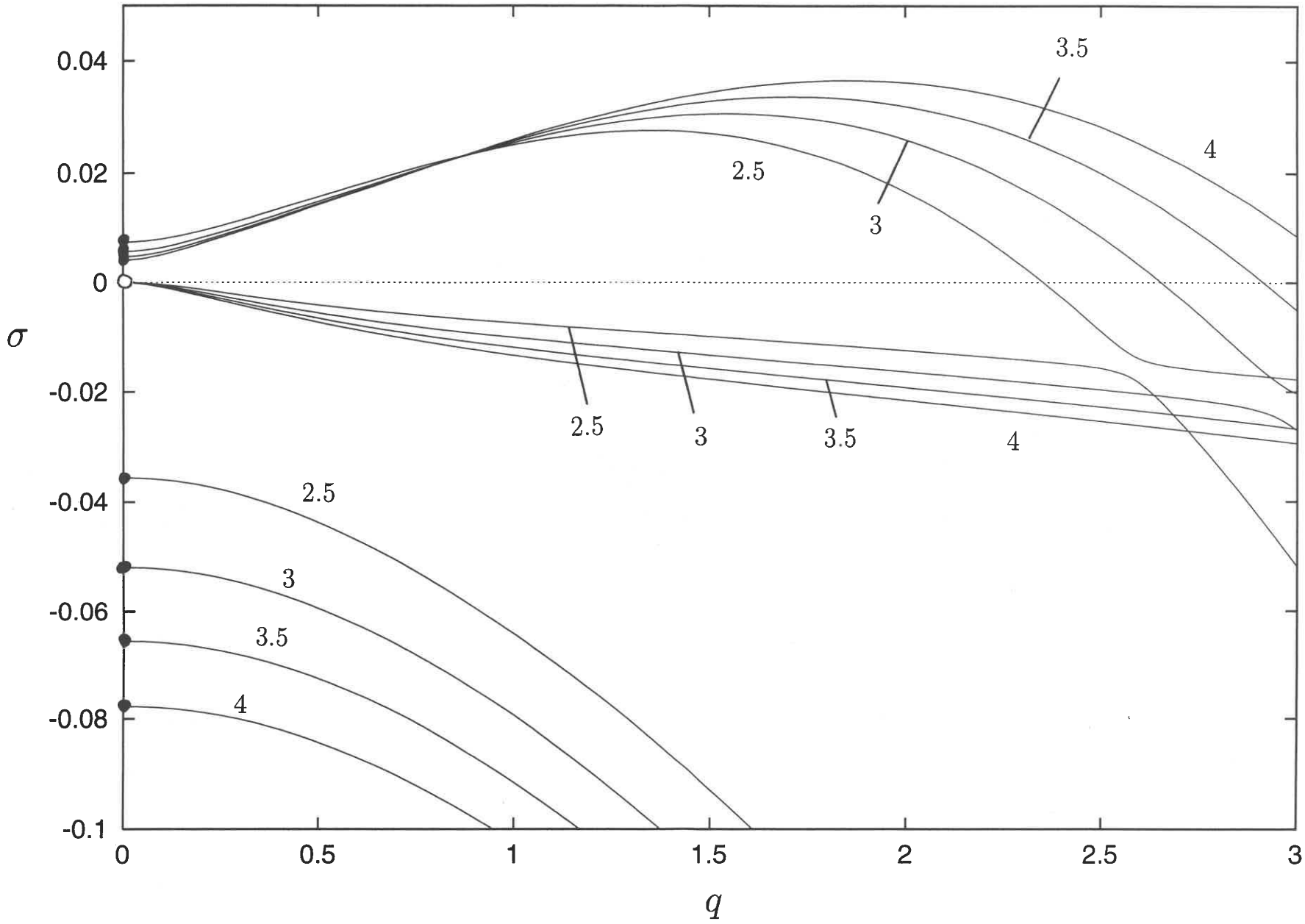

McKinley, Phys. Fluids

Fig. 15

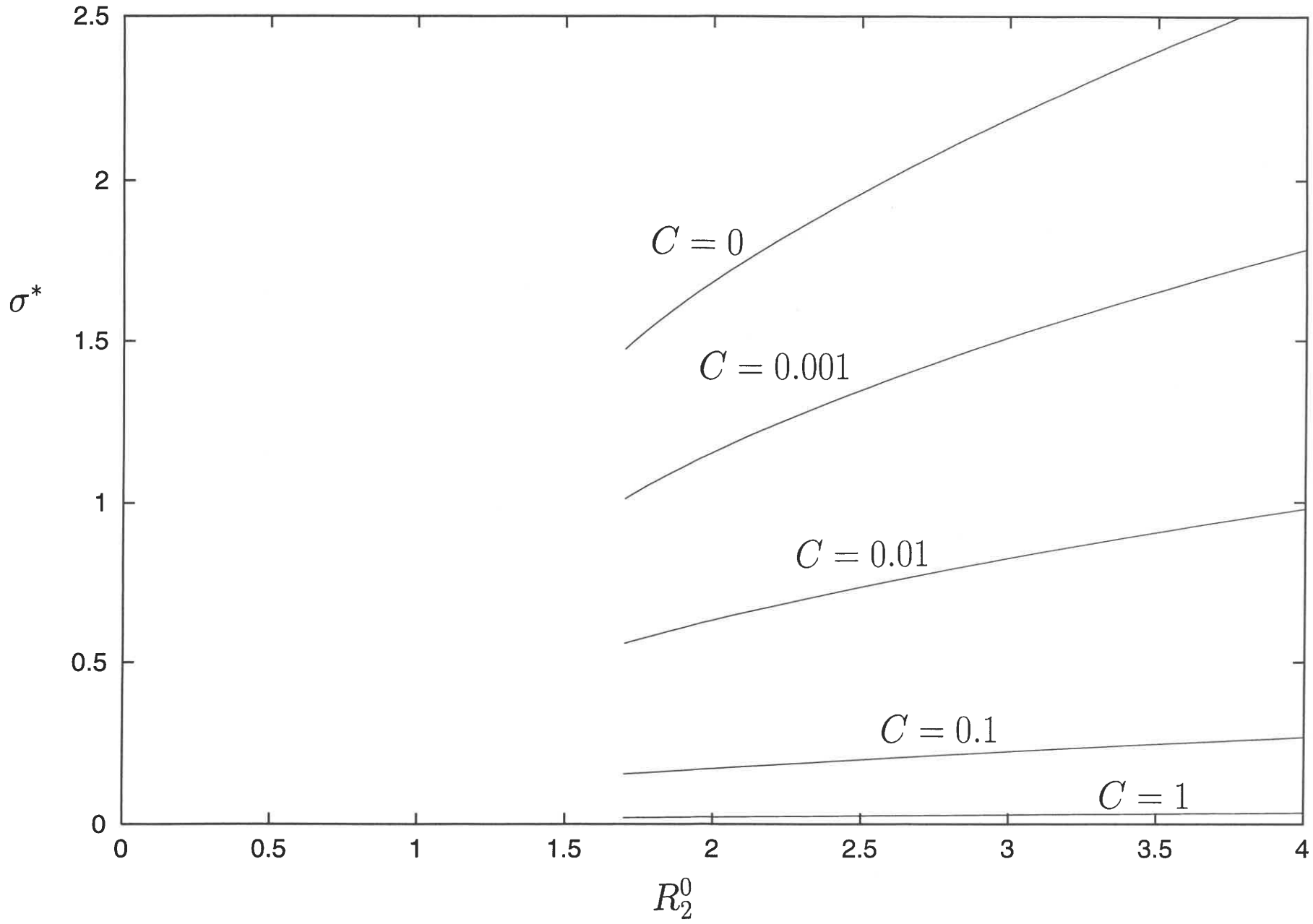

McKinley, Phys. Fluids Fig. 16

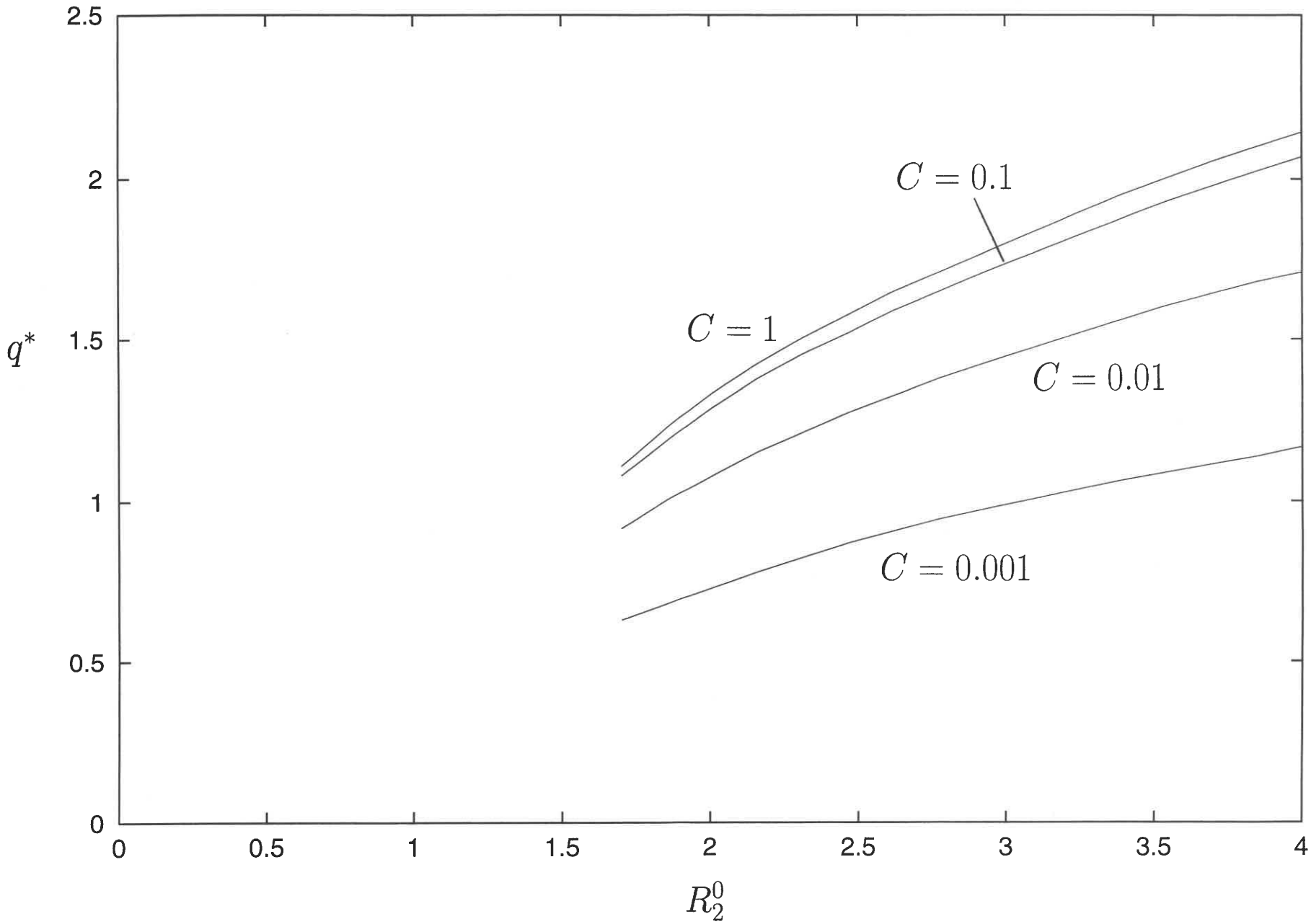

McKinley, Phys. Fluids

Fig. 17